Solid-State Photoemission and Related Methods: Theory and Experiment

W. Schattke, M.A. Van Hove (Eds.)

Wiley-VCH Verlag & Co. KGaA
August 4, 2003

Contents

1 Overview of core and valence photoemission

W. Schattke, M.A. Van Hove, F.J. García de Abajo, R. Díez Muiño, and N. Mannella

1.1 Introduction

This chapter attempts to give a general and systematic introduction to the theory and computation of photoelectron emission from both core and valence levels in surfaces and molecules. Given this subject's long history and ample literature, it is not possible, or indeed necessary, to cover all aspects and contributions here.

It is hoped that this chapter provides a basis for a better understanding of the other contributions in this volume, and that it offers an educational foundation for those wishing to enter or study the field: it is written in particular with the experimentalist and new reader in mind, stressing concepts and omitting detailed derivations.

Figure 1.1 describes the basic principles of photoelectron spectroscopy, illustrating various effects that can take place.

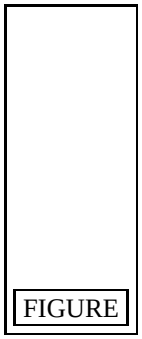

Figure 1.1: Photoemission spectroscopy from a surface, plotted as energy vs. position perpendicular to the surface, with the bulk at left. The curves at right represent measured photoemission yields. The photon energy is $\hbar\omega$. The potentials felt by a photoexcited electron may differ between atoms A and B, even if these are of the same type, as a result of a chemical shift due to the surface.

The treatment of the photoemission process starts here with an introduction to Green function methods, which have found wide and profound applications to address one-particle as well as many-body problems, both analytically and numerically. The notion of Green functions is presented in a step-wise and didactic fashion in Section 1.2, to introduce the language and tools used by many theorists in tackling the relatively complicated many-body problem that underlies processes like photoemission. Simplified models are discussed in relationship

ISBN: 0-000-00000-0

to the more general and accurate description. In particular, the photocurrent expression is decomposed into its basic ingredients: initial state, final state, transition operator (matrix elements). And powerful concepts such as self-energy, quasiparticles and spectral representation are carefully introduced.

The famous Golden Rule is discussed in detail, connecting it with the one-step formulation of photoemission in Section 1.3: the distinction with the three-step formulation is shown to have mainly historical relevance, as it is no longer significant with current methods. The basic photoemission operator is introduced in its various representations and approximations, in particular the dipole approximation, in Section 1.4.

Of great importance for a numerically accurate treatment of photoemission is knowledge of the initial and final electronic states. For the initial state, in which the photoelectron resides before the photoemission process, a clear distinction is drawn between localized levels on the one hand (such as core levels in a solid surface, or any atomic levels in a free atom) and delocalized levels on the other hand (such as valence states in a solid surface or molecule). This is treated in Section 1.5.

The final state describing the photoelectron after excitation can be viewed either in a multiple-scattering representation, or in a band picture in terms of its full wavefunction. Computational methods to efficiently handle these often complicated states are also discussed in Section 1.6.

The photoemission matrix elements are treated in Section 1.7: these combine the initial and final states according to the photoexcitation operator. Again, a distinction is made between core and valence initial states: it is shown in particular how the case of extended states can be reduced to the case of localized states.

Optical effects due to the incoming photons are often neglected in modeling photoemission, in the hope that they are small. Here the focus is on the interaction of the photon with the material before a photoexcitation occurs. Examples include atomic resonances, treatable from a localized point of view (Subsection 1.8.1), and screening as well as plasmon resonances, which need a delocalized treatment (Subsection 1.8.2).

More generally, a variety of optical effects can be treated theoretically and computationally, and can be shown to be quite significant under suitable circumstances. These include short-wavelength local fields, non-local response, higher-order many-body Coulomb terms, and mean-field Fresnel considerations, even within a linear response assumption.

Very useful degrees of freedom in photoemission are the polarization of the incident photons, and the electron spin, usually measured as spin polarization of the outgoing electrons. In particular, these can be very fruitfully combined in studies of magnetism at surfaces and interfaces. They also provide high sensitivity to small effects such as relaxed atomic positions. Relativistic effects also contribute to spin polarization, and are covered as well in Section 1.9.

Finally, the success of the theoretical formalisms is borne out with the help of computational codes: these make it possible to actually compare theory to experiment, in a first stage, and then to extract useful new information from experiment. A number of such codes have been produced, and several of them are advanced enough in their user-friendliness to be distributed for general use by surface and interface scientists, as discussed in Section 1.10.

The subjects covered in this chapter also highlight needs for the future. Topics such as dynamic screening of the electron hole, and inclusion of proper thermal vibrations have been much discussed but not implemented in a systematic way. Also lacking is a proper treatment

of non-linear optical effects, observed with strong incident light; these will become even more important with free-electron lasers. Likewise, there is a need for inclusion of time-dependent effects in the theory, such as occur in pump-probe experiments. To some of these fields detailed reference is found in other chapters of this book.

1.2 Green function methods

1.2.1 Photoemission and the many-body problem

Fundamental to the behavior of a collective system are the interactions between the many participating bodies. The many-body problem can be defined as the study of how the interactions between bodies alters the behavior of the isolated, non-interacting bodies.

The photoemission process in its original concept is viewed as a single-particle probe – two-electron photoemission has been studied only recently (as described in two chapters [30, 36] of this volume). A single electron is removed from its binding environment and its spectral and angular distributions are recorded outside the material. Thus, two questions arise. First, how are the many-body effects on the one-particle spectra isolated so as to yield the simple and accustomed interpretation of one-electron photoexcitation? This asks for a quasi-particle picture, which is the subject of many treatments of many-body theory. Photoemission will directly reflect the distribution of those quasi-particles if the picture works at least in an approximate manner. This is by far the most widespread motivation and application of the technique. The second question is: what can be learned from photoemission about the many-body behavior of the system? The one-electron spectra describe excitations, but these do not necessarily have a quasi-particle-like character. Instead, several particles or even collective modes may mix into the excitations and thus affect the entire photoemission process. Then of course, the simple direct interpretation of spectra breaks down and one of the main advantages of this spectroscopy seems to be lost.

However, excitations of the many-body system clearly can be revealed by photoemission, as with any spectroscopy that couples to the excitation process. The angular-resolution capability of photoemission adds a valuable selection property typical for solid state systems. Thus, it is the many-body excitation spectrum which is hidden in the photoelectron spectral distribution. Investigations have made significant progress toward this goal, including analyses of the many-body spectral density, of the Fermi-liquid type or the shape of the Fermi surface [21, 94], of the intrinsic and extrinsic inelastic losses by plasmon shake-offs [49], and of magnetic excitations [55]. The momentum resolved gap in semiconductors hides many-body effects, and is an experimental quantity that can be extremely carefully determined by photoemission. Theoretical investigations have culminated in the quantitative evaluation of the *GW*-approximation now most common to bandstructure calculations. [37, 59] Strongly correlated systems present another challenging problem of many-body physics [60] where spectroscopy has opened a new branch with two-electron photoemission, see [36].

Thus, the present development of photoemission increasingly requires the treatment of many-body effects. For that reason, we here introduce the main ideas of many-body theory at a relatively basic level, meant to offer non-specialists insight into the main concepts. A more extensive treatment is available in many books. [24, 61, 83] Several chapters of this handbook

will address in much greater detail several aspects that are critical for photoemission and related techniques.

The importance of the many-body problem derives from the fact that almost any property of a real physical system of particles is to some degree governed by the quantum mechanical interactions between the particles themselves. Thus, the many-body problem is not necessarily a branch of solid-state, nuclear or atomic physics. It deals with general methods applicable to all many-body systems. The difficulty of solving the many-body problem is extreme, and because of this not much progress was made for a long time. The simplest way to deal with the many-body problem was simply to ignore it, i.e. to neglect the interactions between the particles of the system (One-Body Approximation). It is surprising and mysterious how this simple picture was able to produce good results nonetheless. An explanation such as 'many-body corrections often arise according to alternating semiconvergent series where subsequent terms tend to cancel, thus wisdom only keeps the lowest order' sounds mysterious as well and asks for examples and proof.

In a series of papers around 1956-57, it was shown that the methods of Quantum Field Theory, already famous for its success in elementary particle physics, were able to provide a powerful, systematic and unified way to attack the many-body problem. One of the most important results emerging from this approach is a new simple picture of matter according to which systems of interacting real particles are described in terms of approximately non-interacting fictitious bodies, called *quasi-particles*, and *collective excitations*. To a large extent, the properties of quasi-particles and the description of the collective excitations can be calculated by means of quantum-field-theoretical techniques pictorially assisted by the so-called Feynman diagrams. Actually, this represents the most general and systematic access to the many-body problem.

The discovery of the Hohenberg-Kohn theorem [56] has sparked a whole "industry" of bandstructure calculations for which photoemission has proved to be the most accurate tool of experimental investigation. The theorem describes the exact ground state energy as a functional of the electron density which is variationally exploited once this functional is known. Various approximations to the latter have been developed with increasing accuracy. Furthermore, in contrast to the fact that only the ground state is covered by the theorem, excitation energies are identified in an approximate way with the constraint parameters of the variational equations, the Kohn-Sham equations [69]. The agreement with experiment widely confirms this procedure in *density functional theory* (DFT). Because of their importance, many-body treatments can no longer be considered separately from DFT. It is well known [99] that the Kohn-Sham equations can be regarded as a procedure to solve the exact Dyson equation for Green functions with a suitable self-energy. Thus, the formulation of many-body theory with Green functions embeds DFT in its most frequently applied environment.

The general development of many-body theory for solids proceeds via Green functions and so does photoemission theory. Therefore, Green functions will be the basis of the following presentation. In Section 1.2.2, we will introduce Green functions in the context of the one-particle Schrödinger equation. In Section 1.2.3, we will discuss elementary excitations in systems of interacting particles. Section 1.2.4 will address the concept of the self-energy, while Section 1.2.5 will consider independent particle states and related methods. Perturbation expansions will be discussed in Section 1.2.6, and diagrams in many-body systems will be presented in Section 1.2.7. Section 1.2.8 introduces the spectral representation, while Sec-

tion 1.2.9 deals with the photocurrent.

1.2.2 Green functions and one-particle Schrödinger equation

Let us consider a single quantum mechanical particle with Schrödinger's equation written in Dirac's notation as

$$(E\widehat{I} - \widehat{H}_0)|\psi\rangle = \widehat{V}|\psi\rangle \tag{1.1}$$

Here $\widehat{H}_0$ is a Hamiltonian for which the eigenfunctions ϕ_n and the eigenvalues E_n ($widehatI$, identity operator) are known, while $\widehat{V}$ is a

Such an equation can be solved provided that we know the inverse of the operator $(E\,\widehat{I} - \widehat{H}_0)$, namely the Green function $\widehat{G}_0 = (E\widehat{I} - \widehat{H}_0)^{-1}$ (we will often abbreviate "Green function" to GF). In light of this, we observe that the operators $(E\,\widehat{I} - \widehat{H}_0)$ and $\widehat{H}_0$ share the same eigenfunctions $\phi_n(\mathbf{r})$ since they commute, while the eigenvalues of the operator $(E\,\widehat{I} - \widehat{H}_0)$ are shifted, equal to $E - E_n$. The Green function of the operator $(E\widehat{I} - \widehat{H}_0)$ is therefore brought into the position representation, $G_0(\mathbf{r}, \mathbf{r}', E) =< \mathbf{r}|\widehat{G}_0|\mathbf{r}' >$, by expanding with respect to its eigenfunction system

$$G_0(\mathbf{r}, \mathbf{r}', E) = \sum_n \frac{\phi_n(\mathbf{r})\phi_n^*(\mathbf{r}')}{E - E_n} \tag{1.2}$$

Here we can appreciate a powerful feature of the Green function: by finding the values of the parameter E for which the denominator of the GF vanishes, we can obtain the eigenenergies of the operator $\widehat{H}_0$. This result motivates the use of the GF formalism later on when dealing with the much more complex problem of the interaction of a quantum mechanical particle within an interacting-particle system. In particular, we will see later that in that case the GF has poles at values of the parameter E equal to the excitation energies of the whole system.

By applying the GF operator we get from Eq. (1.1)

$$|\psi\rangle = |\psi_0\rangle + \widehat{G}_0\widehat{V}|\psi\rangle \tag{1.3}$$

where $|\psi_0\rangle$ is the solution of the associated homogeneous equation $(E\,\widehat{I} - \widehat{H}_0)|\psi_0\rangle = 0$. By successive approximations of the particular solution $\widehat{G}_0\widehat{V}|\psi\rangle$ through iteration of Eq. (1.3), it is possible to express the general solution as

$$|\psi\rangle = |\psi_0\rangle + \widehat{G}_0\widehat{V}|\psi_0\rangle + \widehat{G}_0\widehat{V}\widehat{G}_0\widehat{V}|\psi_0\rangle + \cdots \tag{1.4}$$

We can also consider the following problem: if we know the Green function $\widehat{G}_0$ for the operator $\widehat{H}_0$, what is the GF G for the operator $\widehat{H}_0 + \widehat{V}$? By definition,

$$\widehat{G}(E) \;= \left(E\widehat{I} - \widehat{H}_0 - \widehat{V}\right)^{-1}$$

Since $\left(E\widehat{I} - \widehat{H}_0 - \widehat{V}\right)\widehat{G}\,(E) = \widehat{I}$, we have

$$\left(E\widehat{I} - \widehat{H}_0\right)\widehat{G}\,(E) = \widehat{I} + \widehat{V}\,\widehat{G}\,(E) \tag{1.5}$$

and multiplying both sides by $\widehat{G}_0(E)$, we obtain

$$\widehat{G}\,(E) = \widehat{G}_0(E) + \widehat{G}_0(E)\widehat{V}\,\widehat{G}(E) \tag{1.6}$$

which is called *Lippman-Schwinger equation*. Projecting onto the position eigenstates $|\mathbf{r}\rangle$, Eq. (1.3) and the Lippman-Schwinger equation are respectively written as

$$\psi(\mathbf{r}) = \psi_0(\mathbf{r}) + \int G_0(\mathbf{r},\mathbf{r}')V(\mathbf{r}')\psi(\mathbf{r}')\,d\mathbf{r}' \tag{1.7}$$

$$G(\mathbf{r},\mathbf{r}',E) = G_0(\mathbf{r},\mathbf{r}',E) + \int G_0(\mathbf{r},\mathbf{r}'',E)V(\mathbf{r}'')G(\mathbf{r}'',\mathbf{r}',E)\,d\mathbf{r}'' \tag{1.8}$$

Both these equations are integral equations which can be solved up to the desired order by successive iterations. Both formulas find widespread application in multiple scattering theory.

Now we consider the time evolution of a single quantum mechanical particle with unperturbed Hamiltonian $\widehat{H}_0$. Schrödinger's equation in this case can be written as

$$\left[i\hbar\frac{\partial}{\partial t} - \widehat{H}_0\right]|\phi(t)\rangle = 0 \tag{1.9}$$

Projecting onto the position eigenstates, the Green function $G_0(\mathbf{r},\mathbf{r}',t,t')$ of the operator $i\hbar\frac{\partial}{\partial t} - \widehat{H}_0$ satisfies the following differential equation

$$i\hbar\frac{\partial}{\partial t}G_0\left(\mathbf{r},t,\mathbf{r}',t'\right) - H_0\left(\mathbf{r},\frac{\hbar}{i}\nabla\right)G_0\left(\mathbf{r},t,\mathbf{r}',t'\right) = \hbar\delta\left(t-t'\right)\delta\left(\mathbf{r}-\mathbf{r}'\right) \tag{1.10}$$

Equation (1.2) shows that the solution $G_0(\mathbf{r},\mathbf{r}',t,t')$ of Eq. (1.10) is the Fourier transform of the Green function $G_0(\mathbf{r},\mathbf{r}',E)$

$$G_0(\mathbf{r},t,\mathbf{r}',t') = \frac{1}{2\pi}\int G_0(\mathbf{r},\mathbf{r}',E)e^{-\frac{i}{\hbar}E\left(t-t'\right)}dE \tag{1.11}$$

where the zeros of the denominator of the Green function $G_0(\mathbf{r},\mathbf{r}',E)$ are appropriately avoided by suitable choice of an integration path in the complex plane. Equivalently, one integrates on the real axis and moves the zeros off that axis by defining

$$G_0^{r/a}(\mathbf{r},\mathbf{r}',E) = \sum_n \frac{\phi_n(\mathbf{r})\phi_n^*(\mathbf{r}')}{E - E_n \pm i\delta} \tag{1.12}$$

with δ an infinitesimal positive quantity and the sign leading to a retarded (r) or advanced (a) choice(+ or - sign,respectively). It is possible to close the contour of integration in the lower half-plane if $t > t'$ and in the upper half-plane if $t < t'$, so that $G_0^r(\mathbf{r},t,\mathbf{r}',t') = 0$ for $t < t'$ and $G_0^a(\mathbf{r},t,\mathbf{r}',t') = 0$ for $t > t'$. The Green functions $G_0^{r/a}(\mathbf{r},t,\mathbf{r}',t')$ are both solutions of equation (1.10), but with different prescriptions for the boundary condition on the time axis.

Through Eq. (1.10) an interesting property of the Green function shows that, given an arbitrary initial wave function $\phi(\mathbf{r}',t')$ at time t', it is possible to write the solution of the Schrödinger equation at a later time t as

$$\phi(\mathbf{r},t) = i\int G_0^r(\mathbf{r},t,\mathbf{r}',t')\phi(\mathbf{r}',t')d\mathbf{r}' \tag{1.13}$$

as proved with help of Eq. (1.10) and the equal-time property $iG_0^{r/a}(\mathbf{r},t,\mathbf{r}',t) = \delta(\mathbf{r}-\mathbf{r}')$. For this reason G_0^r is called *retarded propagator*: G_0^r "propagates" the wave function through time. The condition $G_0^r = 0$ for $t < t'$ ensures that values $\phi(\mathbf{r}',t')$ for times later than t do not contribute to the determination of $\phi(\mathbf{r},t)$. In this sense the Green function G_0^r and the corresponding *advanced* Green function G_0^a embody the principle of causality.

Now that we have the solutions of the unperturbed Green function Eq. (1.10), we can solve the problem of determining the time evolution for a quantum mechanical particle with Hamiltonian H_0 and with a perturbing potential $\widehat{V}(t)$ which can be time-dependent. In this case the Schrödinger equation can be written as

$$\left[i\hbar\frac{\partial}{\partial t} - \widehat{H}_0\right]|\Psi(t)\rangle = \widehat{V}(t)|\Psi(t)\rangle \tag{1.14}$$

The solution of this equation is obtained by applying the Green function operator on the RHS, so that

$$\Psi(r,t) = \phi(\mathbf{r},t) + \frac{1}{\hbar}\int G_0^{r/a}(\mathbf{r},t,\mathbf{r}',t')V(\mathbf{r}',t')\Psi(\mathbf{r}',t')d\mathbf{r}'dt' \tag{1.15}$$

where $\phi(\mathbf{r},t)$ is the solution of the associated homogeneous Eq. (1.9) and $G_0^{r/a}(\mathbf{r},t,\mathbf{r}',t')$ is the unperturbed Green function which corresponds to $\widehat{V} = 0$. The retarded version yields a *forward* solution, i.e. ϕ is the prescribed initial wave function before the potential $\widehat{V}$ is switched on, and the advanced version yields the *backward* solution, i.e. ϕ is the final wave function after $\widehat{V}$ has been switched off. Replacing in Eq. (1.10) $\widehat{H}_0$ by $\widehat{H} = \widehat{H}_0 + \widehat{V}$ and G_0 by the full Green function G constitutes the differential equation for G and is equivalent to an integral equation, namely

$$\begin{aligned} G^{r/a}(\mathbf{r},t,\mathbf{r}',t') &= G_0^{r/a}(\mathbf{r},t,\mathbf{r}',t') \\ &\quad + \int G_0^{r/a}(\mathbf{r},t,\mathbf{r}'',t'')V(\mathbf{r}'',t'')G^{r/a}(\mathbf{r}'',t'',\mathbf{r}',t')\,d\mathbf{r}''dt'' \end{aligned} \tag{1.16}$$

We notice that by Fourier transforming Eqs. (1.15) and (1.16) into the energy domain we get Eqs. (1.7) and (1.8) in the case that V does not depend on time.

When the particle propagator is expanded in a perturbation series by successive iteration of Eq. (1.6), the structure of the terms can be complicated. The use of GF as propagators is a powerful method to help visualizing the physical picture: we sketch this approach next.

The free propagation of the quantum mechanical particle (in the absence of interactions) can be drawn as a straight line. The effects of the interactions of the particle due to an external potential V are symbolized by open circles with attached broken line, as in Fig. 1.2a. We can now visualize the different orders of the interactions in the perturbation expansion of the propagator as a series of scattering events caused by the potential V. Each term in the perturbation expansion is represented by a diagram, so that each of the lines and circles in the diagrams has a definite factor associated with it. There is a one-to-one correspondence of each diagram with each term occurring in expression (1.6), or, in other words, with each term of the perturbation expansion of the propagator. The result of the infinite sum is the exact propagator depicted by a double line, as in Fig. 1.2b. The first aim of a perturbation theory is to regard

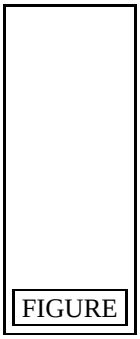

Figure 1.2: Graphical representation of Green function diagrams: a) Green function with zero, one, and n insertions of the perturbing potential; b) graphical summation of the geometrical series up to infinite order to get G

the series as a power expansion with respect to a small parameter which leads to a cut-off at low order.

The perturbation series is sometimes evaluated by summing to infinite order over only a subset of diagrams, that is, summing only over some terms in the perturbation expansion corresponding to certain types of diagrams. This is the so-called *partial* or *selective summation*. The partial sum is usually evaluated by showing that it involves a convergent infinite series, or that it is equivalent to an integral equation which has already been solved.

As an example, consider a quantum mechanical particle which is moving under the influence of the sum of two external potentials V_A and V_B. If such an expansion were summed up to second order according to ordinary perturbation theory, one would retain only five terms: two linear terms (in V_A and V_B) and three quadratic terms (in V_A^2, V_B^2, and $V_A V_B$). If, on the contrary, one of the perturbations cannot be considered small, it is not possible to apply ordinary perturbation theory. For example, if $V_A \gg V_B$, it is possible to consider only the diagrams involving V_A, neglecting V_B and resulting in the "partial" result

$$\begin{aligned}\widehat{G}(E) &= \widehat{G}_0(E) + \widehat{G}_0(E)(\widehat{V}_A + \widehat{V}_B)\widehat{G}(E) \\ &\approx \widehat{G}_0(E) + \widehat{G}_0(E)\widehat{V}_A\widehat{G}_0(E) + \widehat{G}_0(E)\widehat{V}_A\widehat{G}_0(E)\widehat{V}_A\widehat{G}_0(E) + \cdots \\ &= \widehat{G}_0(E) \cdot \sum_{n=0}^{\infty} \left(\widehat{V}_A\widehat{G}_0\right)^n = \frac{\widehat{G}_0(E)}{1 - \widehat{V}_A\widehat{G}_0} = \frac{1}{\widehat{G}_0^{-1}(E) - \widehat{V}_A}\end{aligned} \tag{1.17}$$

It is interesting to note how this approximation and the summation are visualized in terms of diagrams. In particular, the approximation consists in considering only the series pictured in Fig. 1.2a, while Fig. 1.2b shows how the diagrams can be effectively used as a symbolic guide to performing calculations, since they can be manipulated as if they were algebraic quantities.

1.2.3 Elementary excitations in systems of interacting particles

The elementary excitations play a dominant role in the low temperature behavior of a solid, up to room temperature for the electrons. Often, these excitations have quasi-particle properties in the sense that a group of several particles maintains its identity through the course of time and obeys a certain type of statistics, being e.g. of Fermi or Bose character. These quasi-particles have energy and momentum and can thus be treated much like normal particles in theory and experiment. Therefore, it is convenient to discriminate between an excitation which concerns a finite number of particles, such as an electron with its polarization cloud, and an excitation where all the particles are simultaneously involved, so-called *collective* excitations, such as phonons, spin waves, or current-carrying states of superconductivity. Many intermediate forms exist and can be imagined.

For a homogeneous non-interacting system, the energy E versus momentum dispersion relation of a single particle with momentum p and mass m is quadratic, i.e. $E(p) = p^2/2m$. When a real particle moves through a system of interacting particles, its motion is considerably modified. In fact, we can imagine that the real particle becomes surrounded by a cloud of other particles in the system. The system consisting of the real particle plus the cloud of other particles around it is called *quasi-particle*, or synonymously *dressed*, *clothed* or *renormalized particle*. The properties of the quasi-particles are different from those of the real particles: quasi-particles have an effective mass and a lifetime.

Since the real particle is screened by the other particles, quasi-particles interact only weakly with one another. This is why the formulation of the quasi-particle concept is so useful in studying many body systems: systems of strongly interacting real particles may be regarded as composed of independently and/or weakly interacting quasi-particles.

The quasi-particles are what we see when we probe such systems, and they can behave quite differently from the free particles. For example, the energy versus momentum dependence of a quasi-particle can be very different from that of a free particle. Such behavior is what angle resolved photoemission is in fact supposed to elucidate.

We can define quasi-particles as *effective single-particle states*, meaning that they act like free particles with a renormalized energy ϵ'_k replacing the energy ϵ_k of the bare particle, and a lifetime τ_k. In an approximate manner, the finite lifetime of a single-particle state is described by regarding the energy as a complex quantity. By doing so, it is possible to account for the exponential decay in time of the amplitude of the wave function, thus describing the fact that the scattering due to a potential tends to knock a particle out of its single particle state. Thus, we consider the energy with real part equal to ϵ'_k and imaginary part equal to $-1/\tau_k$. In fact, the eigenfunction of a free particle with momentum $\hbar k$ can be written as $\phi_k(t) = \phi_k e^{-i\frac{\epsilon'_k}{\hbar}t}$. When interactions are turned on, the energy changes to ϵ'_k and the particle starts to decay out of the single particle state k , so that for a quasi-particle the wave function can be written as

$$\phi'_k(t) = \phi_k e^{-i\left(\frac{\epsilon'_k}{\hbar} - i\frac{1}{\tau_k}\right)t} = \phi_k e^{-i\frac{\epsilon'_k}{\hbar}t} e^{-t/\tau_k} \tag{1.18}$$

showing the exponential decay of the state with rate $\frac{1}{\tau_k}$.

The quasi-particles are more or less well defined, depending on the value of the decay time. Schemes like Hartree or Hartree-Fock, which rely on the solution of a one-particle-like Schrödinger equation, local or nonlocal, with hermitean Hamiltonian, conserve the particle

number and thus also the identity of a single particle. The Kohn-Sham eigenvalues of density functional theory also exhibit definite single-particle properties, even though this approach is questionable because it describes only the ground state; however, it is empirically in wide use. An important criterion for the validity of the notion of a quasi-particle is that the lifetime of the quasi-particles has to be longer than the time required to detect the quasi-particle state. Since the many-body interactions scatter the particle out of its single-particle state, a measurement of the lifetime of the state is very useful because it gives insight into the interaction mechanisms.

At the other end of the scale of fictitious particles in a many-body system are the *collective modes* or *collective excitations*. These can be defined as the quanta associated with collective wave-like motion of the system as a whole. Examples of collective excitations include phonons, plasmons and magnons. Collective excitations have particle-like qualities, such as complex energies with finite lifetime. Unlike quasi-particles, however, they are not described in a localized picture.

An important aspect of many-body systems is that of the correlations in particle positions brought about by their mutual interaction, giving rise to coherence effects. Such correlations frequently take the form of screening, that is, the alteration in the effective interaction of a pair of particles brought about by the remaining particles in the system. In fact, the particle in a system cannot distinguish between an external perturbation and an internal potential produced by the response to that perturbation from the rest of the system. A particle reacts not to the external field but to the total field, including the response of all the other particles. The result of allowing the rest of the system to adapt itself is to reduce drastically the effective potential. For example, a given electron in a dense electron gas acts to polarize its immediate surroundings: it pushes other electrons away until its associated screening cloud possesses a charge nearly equal (and opposite) to its own. The quasi-particles (electrons plus screening clouds) interact via an effective short-range interaction of the order of the interparticle spacing, in contrast to the original Coulomb interaction which in principle has infinite range. One of the first big successes of many-body theory was the decomposition of the Coulomb excitations into extended plasma waves and short-ranged screening clouds, the former corresponding to collective excitations and the latter to quasi-particles. [12,77] Charges are locally balanced and the remaining long range interaction ($q = 2\pi/\lambda \to 0$) is connected with wave-like deviations from this balanced charge equilibrium at significantly higher energies corresponding to the classical plasma frequency.

It should be noted that each bare particle is simultaneously the core of a quasi-particle and a transient member of the cloud of several other quasi-particles. Therefore, if one wants to describe a many-body system in terms of quasi-particles, caution is necessary because each particle will be counted more than once. For this reason, the quasi-particle concept is valid provided that one talks about a few quasi-particles at a time (few compared to the total number of particles in the system).

It is convenient to define quasi-particles in terms of an experiment in which one removes or adds a particle in a system, and observes the behavior of this extra particle (or hole) as it moves through the system. This picture is closely related to photoemission, direct and inverse, respectively. It is automatically accounted for in the formal definition of the Green function for a many-body system.

1.2.4 The self-energy

At this point it is natural to ask how we can describe the GF propagator when we consider the many-body interactions which are present in a system of particles. A useful aspect of the one-particle many-body Green function is that it allows retaining a one-particle picture while considering many-body systems. In fact, following Dyson, it is possible to describe the many-body interactions of a single particle by introducing an energy dependent effective potential called *self-energy* $\widehat{\Sigma}(E)$. As the name suggests, the self-energy includes all the particle interaction effects. In other words, the particles of the system are perturbed by the incoming particle in such a way that their motion follows (or "is correlated with") the motion of the incoming particle itself. The incoming particle affects the many-body system, which in turn acts back on the particle, altering its energy. The interactions between the incoming particle and the system take place in a dynamic rather than in a static way, so that the self-energy describes the dynamics of these interactions, i.e. the time dependence of the response of particle motion correlated with the incoming particle. For this reason the self-energy is an external effective potential which is time dependent, and hence energy dependent upon Fourier transforming.

In a crude way, the self-energy might be introduced by the following equation reminiscent of Eq. (1.1) with the potential V replaced by the self-energy $\widehat{\Sigma}$

$$\left(E\widehat{I} - \widehat{H}_0\right)|\Psi\rangle = \widehat{\Sigma}\left(E\right)|\Psi\rangle \tag{1.19}$$

where $\widehat{H}_0$ is a Hamiltonian whose eigenvalues and eigenfunctions are well known, typically taken to be of one-particle form. According to the derivation following Eq. (1.3), the formal solution of Eq. (1.19) is obtained through the corresponding GF which is determined by means of the Lippman-Schwinger equation, now called (when the self-energy is present) *Dyson equation*

$$\widehat{G}\left(E\right) = \widehat{G}_0\left(E\right) + \widehat{G}_0\left(E\right)\widehat{\Sigma}\left(E\right)\widehat{G}\left(E\right) \tag{1.20}$$

The Dyson equation can be solved formally

$$\widehat{G}\left(E\right) = \frac{1}{\widehat{G}_0^{-1}\left(E\right) - \widehat{\Sigma}\left(E\right)} \tag{1.21}$$

This shows how the poles of the GF are moved in energy by $\widehat{\Sigma}$ from those of the non interacting GF $\widehat{G}_0$, thus describing the motion of the particle through the system as a combination of its free motion and all of its interactions with the rest of the system, expressed by the self-energy. Equation (1.20) is depicted in Fig. 1.3, where the double lines are associated with the GF $\widehat{G}\left(E\right)$, while single lines denote the free propagator $\widehat{G}_0\left(E\right)$.

The solution of Dyson's equation is symbolic, meaning that it is possible if we know how to calculate the self-energy $\widehat{\Sigma}$. This task, however, is impossible in full generality. It is possible to calculate it by means of approximations of the many-body interactions which are present in the system. A qualitative look at the methods which allow performing this many-body perturbation expansion will be the object of the next paragraphs. The method of *second quantization* or *occupation number formalism* historically facilitated the development

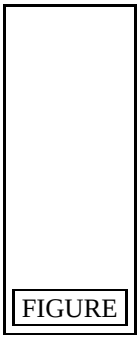

Figure 1.3: Self-energy: a) multiple insertions of self-energy to infinite order for G written in b) by summing them up in Dyson's equation.

significantly. The reason for this is twofold. First, this formalism allows handling systems with variable numbers of particles. This capability can be appreciated if we think about the fact that we will be able to describe test particles which are added to or removed from the system, as embodied in the definition of the GF. As another example, we can formally express the particle-hole approach, where the number of particles and holes is variable. Furthermore, the operators already describe (through the commutation relations that they satisfy) the symmetry properties of Fermi and Bose systems, so that we do not have to worry about keeping the wave functions properly symmetrized, the result being a simplification and a more compact form.

1.2.5 Independent particle states and related methods

It is necessary to use determinantal wavefunctions even for the simplest problems that satisfy the quantum statistics of fermions: such wavefunctions are unwieldy expressions, so it is desirable to find a formalism that is easier to manipulate. The required basic information is how many particles are in the single-particle state α, how many in state β, and so on. In Dirac's notation:

$$|\Psi\rangle = |n_\alpha, n_\beta, \ldots, n_\nu, \ldots\rangle \tag{1.22}$$

In this *number representation* one defines the *construction* and *destruction* operators, $\widehat{c}^\dagger$ and $\widehat{c}$ respectively, to construct a state like Eq. (1.22). They increase and decrease, resp., by one the number of particles in a specified one-particle state $\rho, \sigma, \ldots$. The symmetry properties of the system are implicitly contained in the commutation relations obeyed by these operators, viz.

$$\widehat{c}^\dagger_\rho \widehat{c}^\dagger_\sigma = \pm \widehat{c}^\dagger_\sigma \widehat{c}^\dagger_\rho \qquad \text{or} \qquad \left[\widehat{c}^\dagger_\rho, \widehat{c}^\dagger_\sigma\right]_\mp = 0 \tag{1.23}$$

where we have the anticommutation relation (lower sign) for fermions and the commutation relation (upper sign) for bosons. An independent fermion state is written according to Eq. (1.22) as

$$|\Psi\rangle = (\widehat{c}^+_\alpha)^{n_\alpha} (\widehat{c}^+_\beta)^{n_\beta} \cdots (\widehat{c}^+_\nu)^{n_\nu} \cdots |0\rangle \tag{1.24}$$

by adding particles to the vacuum state $|0\rangle$.

The criterion according to which we write the operator in second quantization is that when operating between two states it gives the same matrix elements as given before in the more classical notation, between two many-particle wavefunctions. As an example, let us consider an operator like

$$\widehat{O} = \sum_{i=1}^{N} \widehat{O}_i \left(\mathbf{r}_i, \frac{\hbar}{i} \nabla_i \right) \tag{1.25}$$

along with its matrix element evaluated between two independent particle states differing by one single-particle wavefunction

$$\langle \rho | \widehat{O} | \sigma \rangle = \int d^3\mathbf{r}\ \phi_\rho^*(\mathbf{r}) O \left(\mathbf{r}, \frac{\hbar}{i} \nabla \right) \phi_\sigma(\mathbf{r}) \tag{1.26}$$

Such operators are called *one-body operators* since they are sums of operators each of which acts separately on one particle. An example of such an operator is the kinetic energy operator. In second quantization formalism, it can be shown that the expression for such operators is given by

$$\widehat{O} = \sum_{\rho\sigma} \langle \rho | \widehat{O} | \sigma \rangle \widehat{c}_\rho^\dagger \widehat{c}_\sigma \tag{1.27}$$

In an analogous way a two-body operator is represented by a product of two destruction and two creation operators and a corresponding matrix element.

Consider again a state in the form of Eq. (1.22) and disregard mathematical subtleties concerning the difference between discrete and continuous states. If we take as the single-particle states α, β, etc. the eigenstates of the position operator $\widehat{\mathbf{r}}_1, \widehat{\mathbf{r}}_2, \ldots, \widehat{\mathbf{r}}_i$, then $n_{\mathbf{r}_i}$ gives the number of particles in the single-particle state $\delta(\mathbf{r} - \mathbf{r}_i)$, i.e., $n_{\mathbf{r}_i}$ particles at the point $\mathbf{r}_i$. Similarly, the creation and destruction operators become $\widehat{c}_{\mathbf{r}_i}^\dagger$ and $\widehat{c}_{\mathbf{r}_i}$, which respectively create and destroy a particle at $\mathbf{r}_i$. These two operators are usually called *field operators* and are denoted by $\widehat{\psi}^\dagger(\mathbf{r}_i)$ and $\widehat{\psi}(\mathbf{r}_i)$, respectively. The exact formal definition of the field operators is by means of linear combination of the creation and destruction operators, namely

$$\widehat{\psi}(\mathbf{r}_i) = \sum_k \widehat{c}_k \psi_k(\mathbf{r}_i)$$

with a suitable set of one-particle states $\psi_k(\mathbf{r})$. From the commutation relations satisfied by the operators $\widehat{c}^\dagger$ and $\widehat{c}$ it is easy to show the respective relations for the field operators. The expressions for the one-body and two-body operators in terms of the field operators become

$$\int d^3\mathbf{r}\ \widehat{\psi}^\dagger(\mathbf{r}) O(\mathbf{r}, \mathbf{p}) \widehat{\psi}(\mathbf{r}) \tag{1.28}$$

$$\iint d^3\mathbf{r}_1 d^3\mathbf{r}_2\ \widehat{\psi}^\dagger(\mathbf{r}_1) \widehat{\psi}^\dagger(\mathbf{r}_2) O(\mathbf{r}_1, \mathbf{p}_1, \mathbf{r}_2, \mathbf{p}_2) \widehat{\psi}(\mathbf{r}_1) \widehat{\psi}(\mathbf{r}_2)$$

where the momentum $\mathbf{p}$ stands for the corresponding *nabla* (∇) expression and applies to its right.

A convenient starting point for a many-body calculation often can be taken from suitable one-body states. The Hartree-Fock (HF) method is a well known example. A determinantal ansatz of single-particle functions is used to minimize the variational energy and thereby fix these functions. The one-body potential might for instance be given by the nuclei's potential $U_{ion}(\mathbf{r}) = -\frac{Ze^2}{4\pi\epsilon_0}\sum_{\mathbf{R}}\frac{1}{|\mathbf{r}-\mathbf{R}|}$ and the two-body potential by the electron-electron Coulomb interaction. The ground state energy E_0 within the HF approximation, summed over electronic states, is given by

$$E_0 = \langle\Psi|\widehat{H}|\Psi\rangle = \sum_a^N \langle a|\widehat{h}|a\rangle + \frac{1}{2}\sum_{a,b}^N \langle ab||ab\rangle \tag{1.29}$$

where we denoted with $\widehat{h}$ the one-electron part of the Hamiltonian, that is, the kinetic energy and the one-body interaction operators. We also have defined

$$\langle ab||ab\rangle = \langle ab|\widehat{V}|ab\rangle - \langle ab|\widehat{V}|ba\rangle \tag{1.30}$$

The first term on the right hand side of Eq. (1.30) is the self-consistent field, while the second one is the exchange term. The HF equations are variationally obtained from Eq. (1.29) by varying the one-particle states involved in the matrix elements. The resulting one-particle states are then occupied according to their corresponding eigenvalues up to a maximum value, the Fermi energy, such that it exhausts the particle number. It is synonymous with the chemical potential in the case of a metal. The Hartree-Fock eigenvalues ϵ_k, referring to the chemical potential μ, are given by

$$\epsilon_k + \mu = \langle k|\widehat{h}|k\rangle + \sum_b^N \langle kb||kb\rangle \tag{1.31}$$

The split-off of the chemical potential from the one-particle energies is common practice in many-body statistical theory and is adopted here, too. At first, these eigenvalues arise as Lagrangian multipliers for norm conservation of the wave function, as in Ritz's variational principle. These eigenvalues get the meaning of one-particle excitation energies known as *Koopman's theorem*. To this end, one subtracts from Eq. (1.29) the corresponding expression with one particle missing and obtains the ionization potential IP, i.e. the energy required to remove from the N-particle ground state a particle occupying a single-particle state. In particular, we have

$$E_k^{N-1} - E_0^N = -\langle k|\widehat{h}|k\rangle - \sum_b^N \langle kb||kb\rangle = -(\epsilon_k + \mu) =: IP(k) \tag{1.32}$$

Therefore, we see that, given an N-particle Hartree-Fock ground state, the energy required to remove a particle in a single-particle state $|k\rangle$ is $-\epsilon_k$. In a similar way, we can consider the process of adding a particle in a single-particle state $|r\rangle$ to the ground state of the N-particle

system. The assumption is that the remaining single particle states remain unchanged. The energy required for this process, the electron affinity EA, is then given by

$$E_r^{N+1} - E_0^N = \langle r|\widehat{h}|r\rangle + \sum_b^N \langle rb||rb\rangle = (\epsilon_r + \mu) =: EA(r) \tag{1.33}$$

The sum of both expressions represents the excitation energy keeping the number of electrons constant. We note that the ionization potential and the affinity usually are positive quantities with suitable choice of the one-particle energy zero.

To solve the Hartree-Fock equations for a solid is quite cumbersome and the validity of the results is questionable. For example, the gap in insulators and semiconductors is sometimes overestimated by well over 100%. The reason is found in the exchange energy which is negative with an absolute value that is too high: this is due to neglect of the Coulomb hole, an electron's neighborhood of charge density reduced by screening. Thanks to the development of the Hohenberg-Kohn theorem, density functional theory (DFT) has become very successful and has almost entirely replaced all other single-particle-like methods. Various levels of accuracy and variants of the density functional are used. Details can be found elsewhere in this handbook [37, 70]. In the first version of the theory, gaps are underestimated by some 10%. This shortcoming is attributed to the failure of the ground state theory to describe excitations. Koopman's theorem does not hold, contrary to Hartree-Fock. Electron-electron interactions are partly present in the formalism, depending on the choice of the density functional, but its more or less local form does scarcely account for the neighboring electron configuration during excitation. Thus, transferring from a bonding to an antibonding state expands the charge which interacts with and changes the neighborhood via electrostatics and exchange, by Coulomb hole and screened exchange contributions. Improvements with respect to *correlation*, i.e. the difference between the true many-body state and the Hartree-Fock state, have been developed. Of course, they generally aim to take many-body corrections into account.

In DFT, the energy

$$E[n] = T[n] + \int d\mathbf{r} V(\mathbf{r}) n(\mathbf{r}) + \frac{e^2}{8\pi\epsilon_0} \int d\mathbf{r} d\mathbf{r}' \frac{n(\mathbf{r}) n(\mathbf{r}')}{|\mathbf{r} - \mathbf{r}'|} + E_{xc}[n] \tag{1.34}$$

has to be minimized under the constraint of particle number conservation with respect to the density n. Square brackets denote functional dependence. The exchange-correlation functional $E_{xc}[n]$ is adapted in an approximate way from its homogeneous electron-gas form, thereby replacing the constant density n_0 by the true density n. The second term on the right of Eq. (1.34) includes the electron-nucleon potential and, if present, an external force. The third term is the classical electrostatic electron-electron interaction. The kinetic energy $T[n]$ can be chosen such that a set of Schrödinger-like equations arises as variational equations, the so-called *Kohn-Sham equations*

$$\left(-\frac{\hbar^2}{2m} \nabla^2 + v_{\text{eff}}(\mathbf{r}) \right) \phi_k(\mathbf{r}) = \epsilon_k \phi_k(\mathbf{r}) \tag{1.35}$$

with an effective one-body potential

$$v_{\text{eff}}(\mathbf{r}) = V(\mathbf{r}) + \frac{e^2}{4\pi\epsilon_0} \int d\mathbf{r}' \frac{n(\mathbf{r}')}{|\mathbf{r} - \mathbf{r}'|} + \frac{\delta E_{xc}[n]}{\delta n(\mathbf{r})} \tag{1.36}$$

The density is given by a sum over occupied states

$$n(\mathbf{r}) = \sum_k |\phi_k(\mathbf{r})|^2 \tag{1.37}$$

which can be solved iteratively to self-consistency together with Eq. (1.35).

1.2.6 Perturbation expansion

To develop a suitable perturbation approach, let us start with the formal definition of the *one-particle many-body time-ordered Green function* G for fermions:

$$\begin{aligned} G(k_1,t_1,k_2,t_2) = \quad & G^+(k_1,t_1,k_2,t_2) = -i\left\langle \Psi_0^N \middle| c_{k_1}(t_1)\, c_{k_2}^\dagger(t_2) \middle| \Psi_0^N \right\rangle,\ t_1 > t_2 \\ & G^-(k_1,t_1,k_2,t_2) = +i\left\langle \Psi_0^N \middle| c_{k_2}^\dagger(t_2)\, c_{k_1}(t_1) \middle| \Psi_0^N \right\rangle,\ t_1 < t_2 \end{aligned} \tag{1.38}$$

Here $c_k^\dagger(t)$ and $c_k(t) = e^{\frac{i}{\hbar}\widehat{H}t} c_k e^{-\frac{i}{\hbar}\widehat{H}t}$ are, respectively, the creation and destruction operators at time t in a single-particle state k. The time dependence used here is attributed to the so-called *Heisenberg representation*. By k we denote a set of quantum numbers like, for example, momentum $\mathbf{k}$ and spin α. An equation analogous to Eq. (1.10) can be derived for G by differentiating Eq. (1.38) with respect to time but with the essential difference that, besides the $H_0 \cdot G$ term in Eq. (1.10), expectation values over more than two particle operators arise, owing to the number of four c-operators in the interaction part of H. They cannot be decomposed into a product of known quantities factoring out G in a closed form. Instead, by definition the self-energy Σ is formally introduced according to Eq. (1.20), while tools must still be developed to determine Σ explicitly. In the single-particle case, however, Eq. (1.38) defines G as obeying Eq. (1.10). The functions $G^\pm$ are also defined by Eq. (1.38), postulating them to be zero outside the ascribed time interval. They merely serve here for short hand notation. They are different from the retarded and advanced functions which are used in Eq. (1.12) for the one-particle case. The latter can be obtained by $G^r = G - G^<$ and $G^a = G - G^>$, respectively, through the quantities $G^>$ ($G^<$) which equal G^+ (G^-) but extend the specific definition (1.38) to the whole time domain. Let us now take a look at the physical interpretation of the above defined quantities.

An inspection of Eq. (1.38) suggests considering G^+ written as $G^+ = -i\langle B|A\rangle$, where $|A\rangle = c_{k_2}^\dagger(t_2)\left|\Psi_0^N\right\rangle$ and $\langle B| = |B\rangle^\dagger = \left(c_{k_1}^\dagger(t_1)\left|\Psi_0^N\right\rangle\right)^\dagger$. Then the many-body GF G^+ describes the following sequence of events. Initially, the system is in its ground state $\left|\Psi_0^N\right\rangle$. A particle is created at t_2 in a single-particle state (sps) k_2. Later on, at time t_1, the system has the added particle in the sps k_1. G^+ is proportional to the overlap of these two states, i.e. the probability amplitude that the system at time t_1, after a particle has been introduced at time t_2 in the sps k_2, has the added particle in a sps k_1, which corresponds to the physical interpretation given already. In an analogous way one obtains G^-, the propagator of a hole. When one wants to calculate the GF of Eq. (1.38), a big challenge lies in the fact that $\left|\Psi_0^N\right\rangle$ is the ground state of the interacting N-particle system, which is impossible to calculate in full

generality. In fact, it would be more convenient to calculate the matrix elements appearing in Eq. (1.38) between the states corresponding to the ground state of the non-interacting N-particle system. In principle, the idea is to start off with a non-interacting system, "switch on" the interactions and wait until the new interacting stationary state has been achieved.

It is possible to arrive at a formula which allows calculating the propagator by successive approximations. To accomplish this, one moves to the interaction picture. So far we have worked within the Schrödinger picture, namely by using the Schrödinger equation as given by Eq. (1.9), with $\widehat{H}$ instead of $\widehat{H}_0$. To solve it approximately in terms of a perturbation expansion with respect to a small quantity one has to split off a relatively small part $\widehat{V}$ of the total Hamiltonian $\widehat{H} = \widehat{H}_0 + \widehat{V}$ and expand. The method is again not limited to simply cutting off the expansion at a certain order, but it allows partial summation over certain subsets which appear to yield dominant contributions to the exact result. This becomes especially clear if single terms diverge at any order for special values of the parameters involved. It indicates an instability which would also appear in the exact expression as some kind of singularity at the radius of convergence given by the special parameter values. The partial summation and also the exact result may even hide this singularity which artificially appears in the single expansion terms, because the derivatives may exist up to some order thereby smoothing the parameter dependence of the summed result. Think e.g. of a geometrical series of terms each diverging at the same special parameter value where, however, the series converges to zero and has by continuation a convergence radius which covers that parameter value.

Therefore, one has to design an expansion scheme such that a power series with respect to $\widehat{V}$ is generated, no matter whether it converges or not. This needs some formal manipulations of the Schrödinger equation where the known time evolution of the unperturbed Hamiltonian $\widehat{H}_0$ is taken into account from the beginning: the correction to this time dependence is formulated as a new evolution equation in the so-called *interaction representation*. In this representation, the wavefunction of the system $|\psi(t)\rangle_I$ is transformed according to

$$|\psi(t)\rangle_I = e^{\frac{i}{\hbar}\widehat{H}_0 t}\,|\psi(t)\rangle \tag{1.39}$$

The time evolution of the states $|\psi(t)\rangle_I$ and operators in the interaction representation are given by

$$i\hbar\frac{\partial}{\partial t}\,|\psi(t)\rangle_I = \widehat{V}_I(t)\,|\psi(t)\rangle_I \tag{1.40}$$

$$\widehat{O}_I(t) = e^{\frac{i}{\hbar}\widehat{H}_0 t}\widehat{O}e^{-\frac{i}{\hbar}\widehat{H}_0 t} \tag{1.41}$$

Thus, in the interaction representation, the interaction wavefunction $|\psi(t)\rangle_I$ satisfies a Schrödinger equation with the Hamiltonian $\widehat{V}_I$, while all operators carry now an explicit time dependence defined by the non-interacting Hamiltonian $\widehat{H}_0$. We can now determine how the functions $|\psi(t)\rangle_I$ evolve with time in the interaction representation. Instead of the wave function we will use the Green function. We will omit the index I in the following, understanding all time dependence taken in the interaction representation.

The definition of the propagator Eq. (1.38) contains as unknown quantities the exact ground state and the time dependence of the Fermi operators through the full Hamiltonian. The transition to the interaction picture splits off the perturbation in a way similar to the procedure in the wave equation, see Eq. (1.40). The time dependence is then composed of the bare

Hamiltonian via $\widehat{H}_0$ and a complicated correction which involves $\widehat{V}$. The latter is expanded in terms of $\widehat{V}$. The unknown ground state is dealt with in an analogous manner and reduced to the corresponding ground state of the unperturbed system by means of the adiabatic hypothesis. It consists in assuming that the interacting ground state is obtained from the bare ground state by switching on the interaction infinitely slowly, i.e. adiabatically or without change of energy. It turns out that a very convenient representation of the many terms of the different series occurs, through the time ordering which is denoted by $\widehat{T}$. All factors appearing after that operator have to be ordered in an ascending time sequence from right to left. Thus, one gets an expression for the GF in the form of a perturbation expansion, with the advantage that the matrix elements have to be evaluated between unperturbed ground state vectors of a many-body system. Such matrix elements consist of terms like $\langle \Phi_0 | \widehat{T} \left\{ \widehat{A}_1 \ldots \widehat{A}_n \right\} | \Phi_0 \rangle$, where the operators $\widehat{A}_i$ are creation or destruction operators for particle and holes in the interaction representation. The propagator of Eq. (1.38) then reads

$$G(k_1, t_1, k_2, t_2) = -i \sum_{n=0}^{\infty} \frac{1}{n!} (-\frac{i}{\hbar})^n \int_{-\infty}^{\infty} dt'_1 \int_{-\infty}^{\infty} dt'_2 \ldots \int_{-\infty}^{\infty} dt'_n \qquad (1.42)$$
$$\left\langle \Phi_0 \left| \widehat{T} \left\{ \widehat{V}(t'_1) \widehat{V}(t'_2) \ldots \widehat{V}(t'_n) \widehat{c}_{k_1}(t_1) \widehat{c}^{\dagger}_{k_2}(t_2) \right\} \right| \Phi_0 \right\rangle^C$$

The matrix elements are evaluated by using *Wick's theorem* which states that such an expectation value over a product of creation and destruction operators can be decomposed into a product of expectation values of pairs each containing one creation and one destruction operator, i.e. the unperturbed propagators arise. Take Eq. (1.38), replace the true state Ψ_0 by the unperturbed state Φ_0, and use for the time dependence of the operators the unperturbed Hamiltonian $\widehat{H}_0$. A detailed explanation of the mathematics which allow calculating the matrix elements in a systematic way are beyond the scope of this introduction , see e.g. references [33, 80]. We want to stress, however, that to each term in the series expansion corresponds a proper diagram. In particular, some of the diagrams can be divided into different unconnected pieces, and for this reason they are called *disconnected diagrams*. It is possible to show that only connected or linked diagrams must be taken into account in the evaluation of the propagator, according to the so-called *linked cluster theorem*. That is indicated by the superscript C.

There is an alternative method to derive the perturbation expansion which is entirely equivalent to the above, and also frequently used. The association of Eq. (1.38) with the notion of a Green function as developed in the foregoing paragraphs is more suggestive in that procedure. Briefly, the method uses an equation of motion for the quantity (1.38) obtained from the time dependence of the creation and destruction operators in the Heisenberg representation. A four-operator product appears on the right hand side of this equation within the expectation value bracket. The time evolution of that higher order Green function yields in turn successively higher orders, leading to a hierarchy of equations with an increasing number of operators in the expectation value for the higher-order Green functions. The equation of motion has a structure formally equal to Eq. (1.10), thus suggesting the notion of a Green function. The diagrammatic expansion also follows the rules given below. However, the reasoning for approximations differs occasionally. What appears as a summing up of a subseries of the whole expansion in the language of diagrams is a decoupling or factorization of a higher-order Green

function into lower-order ones.

1.2.7 Diagrams in many-body systems

We already introduced some diagrams in the case of a single quantum mechanical particle and introduced the concepts of selective summation. Here we extend the treatment to a system of N particles. The unperturbed Hamiltonian $\widehat{H}_0 = \sum_n < n|h|n > \widehat{c}_n^\dagger \widehat{c}_n$, is assumed diagonal in the single particle states, say of the one-particle potential of a solid. As $< \Psi_0^N|$ and $|\Psi_0^N >$ in Eq. (1.38) are the same states (fully occupied up to the Fermi surface), G_0 is diagonal in the configuration index n, as well. We now focus on a two-body particle-particle interaction. In second quantization the interaction terms have the form of the two-body operator $\widehat{V}_I = \frac{1}{2} \sum_{k,l,m,n} \langle kl|V|mn\rangle \widehat{c}_k^\dagger \widehat{c}_l^\dagger \widehat{c}_n \widehat{c}_m$, where the matrix element $\langle kl|V|mn\rangle$ involves four single-particle states. Such a matrix element describes the interaction between two particles or holes which, starting as single-particle states ϕ_m and ϕ_n, collide and scatter into the single-particle states ϕ_k and ϕ_l, respectively. This expression for $\widehat{V}_I$ has to be inserted in Eq. (1.42). Applying Wick's theorem as indicated will yield a sum of products of bare propagators $G_0\,(l_2, t_2, l_1, t_1)$ which are characterized by two time and two configurational indices.

The book-keeping of the whole series expansion is now illustrated by diagrams and rules governing their construction, their manifold, and the quantitative expression in Eq. (1.42) associated with them. Instead of Fourier transforming to energies, the original time variables are used here. The propagator G_0 is drawn as a line with the endpoints 1 and 2 whose notation comprises occasionally both space and time variables, cf. Fig. (1.4). Each of these points is connected through the indices with an interaction matrix element, with the exception of the outer indices belonging to the left hand side of Eq. (1.42). The matrix element is plotted as a wavy line. It actually has four endpoints (connections) according to the indices of $\langle kl|V|mn\rangle$. They are grouped pairwise such that (k, m) and (l, n) are at opposite ends of the wavy line, with (m, n) on one side of the line and (k, l) on the other. One can think of the pair (k, m) as belonging to one particle and (l, n) to the other. For example, two matrix elements appear in Fig. (1.4c) associated with a wavy line, the left one with indices $\langle k_1 m|V|kl\rangle$ and the right one with $\langle kl|V|k_2 m\rangle$. The connecting points are called vertices and their indices are summed or integrated over, depending on whether the index labels discrete configurations or a continuous time, respectively. There is only one time associated with each wavy line. The perturbation series for the single particle propagators are built as the sum of all possible different connected diagrams which can be constructed with the basic two-body forces interaction diagram. Such diagrams illustrate how the many body interactions which take place in the system modify the single particle or hole propagators. There is a one to one correspondence between each of these diagrams and each of the terms in the perturbation series expansion. Besides the general case where one does not distinguish between different orders of time, diagrams can be ordered by time: this involves the explicit notation giving the time relation in the propagator, i.e., the notation with particle and hole propagators. Both pictures are valuable and used below.

We will limit our attention to some of the main diagrams which are obtained in the lowest order of approximation for the particular case of the single particle propagator. When ordered

by time a particle diagram is drawn such that the particle enters at the start of a line, undergoes all the possible interactions with the background and then leaves at the end of a line. There are only two first order diagrams, corresponding to $n = 1$ in Eq. (1.42). The first diagram, shown in Fig. (1.4a), describes the direct interaction of the particle with any particle n of the background. One line leaves and enters at the same point, a so-called loop. It means equal times in that propagator.

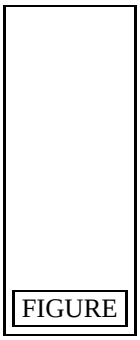

Figure 1.4: First order a) and b), second order c) Coulomb interaction graphs, instead of space momentum variables are denoted in b) and c); only GF indices are shown, matrix elements are e.g. $\langle 1n|V|2n\rangle$, $\langle k_1 l|V|lk_2\rangle$ in a), b), resp..

A propagator associated with a single loop represents the particle/hole occupation number. If the configuration index denotes the momentum of a homogeneous system and if the bare ground state is the free-electron Fermi sphere, then the vertex of the loop has two equal momentum indices, i.e. momentum does not change at one end of the interaction. If momentum is conserved, as e.g. in the Coulomb interaction, then also at the other end no change of momentum can occur. The second process, shown in Fig. (1.4b), corresponds to a particle which undergoes *exchange scattering* against the background particles.

In second order, which means that there are two interactions, the particle propagator can be affected by several scattering processes. A well known and very important type of diagram is shown in Fig. (1.4c), and corresponds to the polarization of the background particles due to the perturbation induced by the incoming particle. Initially the particle (k_1) propagates freely, and then it interacts with the background particles by creating a particle-hole pair (lm). The original particle (now k) and the created particle-hole pair propagate free from interactions, until a new scattering interaction with the original particle annihilates the pair, so that the background returns to its original ground state. This diagram is a non-trivial example of self-energy diagrams. Such diagrams must be considered as an indirect interaction of the particle via the medium with itself. The particle creates a disturbance in the system (interaction) which is then reabsorbed by the particle as it propagates.

We have already pointed out how Dyson's Eq. (1.20) changes the problem of calculating the single particle GF into one of calculating the self-energy. Thus, rather than calculating the whole propagator series, the solution of the problem can be attempted by calculating the self-energy contribution starting directly from the diagrams, and then converting them into an analytical form.

We now illustrate qualitatively the use of Feynman's diagrams in expanding the self-energy. This process is the selective or partial summation, which is equivalent to performing an infinite summation on a series of terms which may even be divergent: in an extreme case, this can produce a new series in which all terms are finite. The original perturbation series usually are not convergent even if the single terms are finite, mostly they are only semiconvergent (asymptotically convergent). Thus they give only a formal representation of the exact expression. One tries to remedy both possible defects, lack of convergence and infinite values of individual terms of the series, by partial summation, which may involve reordering, cancellation of individual terms or cancellation of an infinite number of terms. Not only is the summation performed on self-energy diagrams, but also the interactions themselves are renormalized. This is equivalent to considering effective interactions rather than bare ones. The physical meaning of the effective interactions is that the bare interaction virtually polarizes the medium, and the polarization cloud in turn shields the bare interaction converting it to the much weaker effective interaction. The screened interaction between two points consists of a large number of excitations involving many electron-hole pairs, thus involving the system as a whole.

The diagrams describing the terms in the perturbation expansion can be divided into two classes: reducible (improper) and irreducible (proper). Reducible diagrams can be divided into two by cutting one internal fermion line as e.g. the last two diagrams in Fig. 1.3a, while irreducible ones cannot, as those in Fig. 1.4.

First we attempt to calculate the self-energy. We define as a self-energy part any diagram without external lines, which can be inserted into a particle or hole line. The solution of the Dyson equation is exact, in the sense that all the diagrams have been counted, proper ones and their repetitions. The repetitions appear through the iteration of the Dyson equation; the proper diagrams are to be contained already in the self-energy. Thus, the self-energy must not contain improper diagrams. In principal, it is possible to sum over all repetitions of all irreducible self-energy parts. We have actually shown this process already in Fig. 1.3a. We have only summed over the repeated proper parts, but we still need to sum over the proper parts themselves. This is impossible in full generality, and is normally done with approximations. Understanding which diagrams have more weight in the self-energy expansion is actually challenging: such choice in fact reflects the approximations which are used to describe the system. In other words, choosing the right diagrams to sum over when expanding the self-energy is equivalent to outline the most important physical interactions which take place in a many-body system.

As we associate the full propagators to the straight lines instead of just G^+ or G^-, we have a particle line for the positive time difference, and a hole line otherwise. By suppressing the time order, the drawing of the diagrams can be greatly reduced to their topological equivalence and without any time arrows.

Now we look at the interactions. We define as proper or irreducible polarization part any diagram without external interaction lines which can be inserted into an interaction line and which cannot be split into two by cutting an internal interaction line. When we include all the possible polarization parts, we get the fully screened interactions, as diagrammatically sketched in Fig. 1.5. This procedure is called the dressing or renormalization of the interaction. As an effect of the renormalization, no interaction lines have inserted polarization parts and all interaction lines are dressed. Moreover, as shown in Fig. 1.5b, the interactions obey an equation with the same structure as Dyson's equation, obtained by summing the bare

interaction lines with all the possible insertions of proper polarization parts.

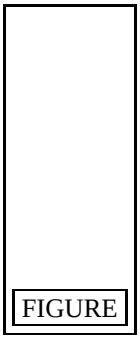

Figure 1.5: Renormalization of interaction by polarization diagrams: a) contributions to polarization, first two graphs are irreducible, third is reducible decomposing into two irreducible ones by cutting the interaction right of the left bubble and has to be removed from a) because it automatically appears in b); b) analog of Dyson equation for interaction.

So far we have seen that the series for the propagator can be expressed in terms of the proper self-energy Σ which can in turn be expressed in terms of the effective interactions. As in Fig. 1.3 we also dress propagator lines. In fact, the self-energy Σ is obtained by summing over all diagrams in which the propagator lines already contain the self-energy. This produces a series in which no propagator lines can be grouped into self-energy parts and all of them have been replaced by clothed propagators.

A vertex is defined as any point in a diagram determined by the intersection of two fermion lines and one interaction line. Then, the vertex part is any diagram without external lines which can be inserted in place of a vertex. The summation for the vertex part can be decomposed in a procedure analogous to renormalization into an irreducible part and its repetition. The lowest order vertex is just a point with three plug-ins, one for the interaction and two for fermions. Any approximation beyond the bare point is called vertex correction.

Altogether, it would be the aim to renormalize simultaneously the interactions, the propagators and the vertices. In the literature the double lines are often omitted, and it is stated that both the interactions and the propagator lines have been renormalized. The whole procedure sketched above produces a large simplification of the book-keeping, illustrating the series expansion of Eq. (1.42).

1.2.8 Spectral representation

We now show how the Green functions $G^{\pm}$ can be expressed in a form which is related to the excitation spectrum of the full Hamiltonian.

By inserting in the definition of the Green function, Eq. (1.38), the unity operator $I = \sum_{n,M} \left|\Psi_n^M\right\rangle \left\langle\Psi_n^M\right|$ (here, n denotes excited states of an M-particle system), we have with $t_1 = t$, $t_2 = 0$ and $k_1 = k_2 = k$

$$G^{+}(k,t) = -i\theta(t) \sum_n |\langle\Psi_n^{N+1}|\hat{c}_k^{\dagger}|\Psi_0^N\rangle|^2 e^{-\frac{i}{\hbar}(E_n^{N+1}-E_0^N)t} \tag{1.43}$$

After Fourier transforming, we get an expression very similar to the one-particle case treated before, namely

$$G^{+}(k,E) = \sum_{n} \frac{|\langle \Psi_n^{N+1}|\widehat{c}_k^{\dagger}|\Psi_0^N\rangle|^2}{E-(E_n^{N+1}-E_0^N)+i\delta} \tag{1.44}$$

Similarly, we get G^{-} with $M = N-1$ for hole creation, with negative imaginary part in the denominator, and with opposite sign of the energies within the parentheses of the denominator. As already pointed out earlier, the poles of the single particle propagator occur at the difference between the exact energy of the excited states of the $N \pm 1$-particle system and the exact ground state energy of the N-particle system. By introducing the $N \pm 1$ ground state energies $E_0^{N\pm1}$ and referring the total excitation energies to them, we obtain ε_n^{N+1} and ε_n^{N-1}. We define the *chemical potentials* $\mu^{N\pm1}$ of the N- and $N-1$-particle systems, respectively, by

$$E_0^{N+1} - E_0^N = \mu^{N+1}, \qquad E_0^N - E_0^{N-1} = \mu^{N-1} \tag{1.45}$$

These are assumed to be independent of the particle number for large N. Thus we have for G, see Eq. (1.38),

$$\begin{aligned} G(k,E) &= G^{+}(k,E) + G^{-}(k,E) \\ &= \sum_{n} \frac{|\langle \Psi_n^{N+1}|\widehat{c}_k^{\dagger}|\Psi_0^N\rangle|^2}{E-\varepsilon_n^{N+1}-\mu+i\delta} + \sum_{n} \frac{|\langle \Psi_n^{N-1}|\widehat{c}_k|\Psi_0^N\rangle|^2}{E+\varepsilon_n^{N-1}-\mu-i\delta} \end{aligned} \tag{1.46}$$

The structure of the denominators in $G^{\pm}$ accounts for the widespread application of the GF formalism in spectroscopy. In fact, we can see that the poles of the GF G^{+} and G^{-} give, respectively, the affinities and the ionization potentials of the N-particle system. Thus, a minimum $\varepsilon_n^{N\pm1} = 0$ refers to the lowest affinity and ionization potential in a conduction band of a metal. In particular, we may consider the conservation of energy for the photoemission process,

$$h\nu + E_0^N = \varepsilon_{\text{kin}} + E_n^{N-1} \tag{1.47}$$

where $h\nu$ is the photon energy and ε_{kin} the kinetic energy of the photoelectron. We write W for $-\mu$, the work function, represented by the vacuum barrier. The binding energy of the photoelectron is then given by

$$\varepsilon_b = h\nu - \varepsilon_{\text{kin}} - W = E_n^{N-1} + \mu - E_0^N = \varepsilon_n^{N-1} \tag{1.48}$$

so that ε_b yields a measure of the excitation energies for the $N-1$-particle system. Note that it is defined as a positive quantity.

It is interesting to evaluate the many-body GF of Eq. (1.46) in the case of a system described in the Hartree-Fock approximation. Again we are assuming that the remaining single particle states remain unchanged in the process of adding to or subtracting a particle from the N-particle ground state, so that we can approximate the final states of the $N+1$- and $N-1$-particle systems as $|\Phi_n^{N+1}\rangle = \widehat{c}_n^{\dagger}|\Phi_0^N\rangle$ and $|\Phi_n^{N-1}\rangle = \widehat{c}_n|\Phi_0^N\rangle$, respectively. Thus the GF of Eq. (1.46) becomes

$$G(k,E) = \sum_{n} \frac{|\langle \Phi_0^N|\widehat{c}_n\widehat{c}_k^{\dagger}|\Phi_0^N\rangle|^2}{E-\varepsilon_n^{N+1}-\mu+i\delta} + \sum_{n} \frac{|\langle \Phi_0^N|\widehat{c}_n^{\dagger}\widehat{c}_k|\Phi_0^N\rangle|^2}{E+\varepsilon_n^{N-1}-\mu-i\delta} \tag{1.49}$$

Measuring the energy with respect to the chemical potential, $\epsilon := E - \mu$ and introducing $\varepsilon_n^{N+1} = \epsilon_k > 0$, $\varepsilon_n^{N-1} = -\epsilon_k > 0$ for the Hartree-Fock energies ϵ_k of particles and holes, respectively, we obtain

$$G(k,\epsilon) = \frac{\theta(k-k_F)}{\epsilon - \epsilon_k + i\delta} + \frac{\theta(k_F-k)}{\epsilon - \epsilon_k - i\delta} \tag{1.50}$$

We thus retrieve Koopman's theorem, according to which the value of $\epsilon_k + \mu$ are the affinity and the binding energy of the system for $k > k_F$ and $k < k_F$, respectively. It is interesting to note that both residues around the poles are equal to one and the imaginary part goes to zero, reflecting the fact that these are exact single particle states with infinite lifetime.

As regards the photoemission process, it is of fundamental importance to observe that the derivation of Eq. (1.50) is based on the assumption that $|\Phi_n^{N-1}\rangle = \widehat{c}_k|\Phi_0^N\rangle$, that is, in the process of subtracting from the N-particle ground state a particle in the sps k, the remaining single-particle states remain unchanged. This is the reason why Koopman's theorem provides the binding energies in the so called *frozen-orbital approximation*, meaning that only the sps state k is considered "active" in the photoemission process, while the other $N-1$ electrons are "passive" spectators, "frozen" in their original single-particle states.

The main ingredient which is neglected in the frozen-orbital approximation is the fact that when a photoelectron in a sps k is emitted from a N-particle system, the remaining $N-1$ electrons relax into a new energy state with energy lower than the Hartree-Fock energy E_n^{N-1} by an amount equal to δE_{relax}, called *relaxation energy*. As a result of neglecting the relaxations, such calculations tend to over-estimate the binding energy. Moreover, Koopman's theorem must be corrected with the electron-electron *correlation effects* which are obtained in going beyond the HF approximation and which reduce the total energy from its HF value.

The *correlation energy* is defined as the difference between the exact energy and the one calculated with Hartree-Fock, namely $E_{\text{corr}} = E_{exact} - E_{HF}$. The correlation energies must be considered for both the initial and the final states, and they are larger in absolute value for systems with higher particle number. Since the correlation energies are negative, the net contribution to the binding energies from correlation effects is positive, i.e. $\delta E_{\text{corr}} = E_{\text{corr}}^{N-1} - E_{\text{corr}}^{N} > 0$.

Therefore, taking into account relaxation and correlation effects, the correction to the expression of the binding energies obtained by Koopman's theorem is given by

$$\varepsilon_k = -\epsilon_k - \delta E_{\text{relax}} + \delta E_{\text{corr}} \tag{1.51}$$

We notice that the corrections due to relaxation effects and correlation effects tend to cancel each other out, so that Koopman's theorem provides a reasonable approximation for the binding energies in photoemission. Striking counterexamples are presented by insulators whose HF gaps are significantly overestimated.

We now define the *spectral density functions*:

$$A^{\pm}(k,\epsilon) = \sum_n \left|\left\langle \Psi_n^{N\pm1} \left|\widehat{a}\right| \Psi_0^N \right\rangle\right|^2 \delta\left(\epsilon - \varepsilon_n^{N\pm1}\right) \tag{1.52}$$

Here $\widehat{a}$ stands for $\widehat{c}_k^{\dagger}$ or $\widehat{c}_k$, respectively, for the upper or lower sign. The spectral density functions are obviously positive, vanish for $\epsilon < 0$, and are related to the momentum distribution

function $\langle n_k \rangle = \left\langle \Psi_0^N \left| \widehat{c}_k^\dagger \widehat{c}_k \right| \Psi_0^N \right\rangle$ through

$$\int_0^\infty dx A^+(k,x) = 1 - \langle n_k \rangle \,, \qquad \int_0^\infty dx A^-(k,x) = \langle n_k \rangle \,, \tag{1.53}$$

From this the *sum rule* immediately follows:

$$\int_0^\infty dx \left[A^+(k,x) + A^-(k,x) \right] = 1 \tag{1.54}$$

We can represent the Green function of Eq. (1.46) with the help of the spectral functions, namely

$$G(k,\epsilon) = \underbrace{\int_0^\infty dx \frac{A^+(k,x)}{\epsilon - x + i\delta}}_{G^+} + \underbrace{\int_0^\infty dx \frac{A^-(k,x)}{\epsilon + x - i\delta}}_{G^-} \tag{1.55}$$

which in turn yields the spectral functions via

$$A^\pm(k,\epsilon) = \mp \frac{1}{\pi} \operatorname{Im} G(k, \pm\epsilon), \quad \epsilon > 0 \tag{1.56}$$

Thus, the Green function G contains the particle as well as the hole spectrum whereas each spectral function A^+ and A^- is associated with only one spectrum. For free particles the spectral density is a δ-function

$$A^\pm(k,\epsilon) = \theta(\pm k \mp k_F)\, \delta\left(\epsilon - \varepsilon_n^{N\pm 1}\right) = \theta(\pm k \mp k_F)\, \delta(\epsilon \mp \epsilon_k) \tag{1.57}$$

that is, the spectral functions are δ-functions at the energies of the single-particle states. In other words, if we are able to detect single-particle states in the system, these must have a spectral function which is a δ-function. Therefore, quasi-particles, which are effective single-particle states, must have a spectral function which resembles a δ-function, like a single peak. We can imagine any curve resembling a sharp peak as being composed of a quasi-particle peak plus a background. We can then make use of Eq. (1.55) with a spectral function which is not a δ-function any more but function with a certain width centered around the peak position. The spectral function dominates in the integral, and it may be assumed that the peak can be represented as a Lorentzian line, i.e. two complex conjugate poles at a quasi-particle state $\epsilon'_k \pm i\Gamma$ with peaked contribution in A^+ and at a quasi-hole state $-\epsilon'_k \pm i\Gamma$ peaked in A^-. If we write the spectral functions as

$$A^\pm(k,\epsilon) = \theta(\epsilon) \frac{1}{\pi} \frac{\Gamma Z}{(\epsilon \mp \epsilon'_k)^2 + \Gamma^2} + \text{background} \tag{1.58}$$

then Eq. (1.55)yields the following Green function through contour integration – both parts G^+ and G^- complete the full real axis and of the poles at $\pm i\Gamma$ only that one is picked up which belongs to the imaginary half-plane opposite to that of the pole characterized by the infinitesimal δ in Eq. (1.55):

$$G(k,\epsilon) = \frac{Z}{\epsilon - \epsilon'_k + i\Gamma \operatorname{sign}(\epsilon)} + \text{background} \tag{1.59}$$

Note again that $\epsilon'_k > 0$ holds for the particle case with A^+ carrying the peak contribution, and $\epsilon'_k < 0$ for the hole case with A^-. We can view Z as the residue of $G^{\pm}$, the so-called renormalization constant. It represents the spectral weight of the dominant structure, the remaining background being smooth. Since $A^{\pm}(k,\epsilon)$ obeys the sum rule of Eq. (1.54), $Z < 1$ follows, because the first term in Eq. (1.58) integrates to Z and the positive background accounts for the difference from unity according to the sum rule. Equation (1.59) reflects the fact that the quasi-particle is a single-particle state with a probability less than unity. The quantities Γ and Z may depend on k as well as on ϵ, because they derive from the self-energy, the more important dependence owing to $\Gamma(\epsilon)$. For example, if $\Gamma(\epsilon)/\epsilon \to 0$ for $\epsilon \to 0$ in approaching the Fermi energy, the right part Eqs. (1.53) and Eq. (1.58) reveal that $< n_k >$ vanishes from above ($\epsilon'_k = 0^+$) and coincides with Z from below ($\epsilon'_k = 0^-$). Thus the Z is equal to the discontinuity of the momentum distribution function at the Fermi level: as expected, the discontinuity is equal to 1 for a noninteracting system, where the Fermi function is a θ function at $T = 0$ which drops discontinuously to zero, and it is less than 1 (and the step function gets partly smeared) when the interactions are turned on. A particle peak of finite width above the Fermi sea is not entirely confined to above the tail leading to a finite hole occupation below. That is reflected according to Eqs. (1.53) and (1.58) by non-vanishing $A^-(k,\epsilon)$ for $\epsilon'_k > 0$ with $\epsilon > 0$. A finite value of Γ shows a finite lifetime of the quasi-particle state. Investigating many-body effects such as in strongly correlated systems photoemission spectra predominantly are interpreted in terms of quasi-particle energies and the spectral function, which seduces because of its simplicity bearing the danger of misinterpretation, however. [39] The actual photoemission analysis becomes a little delicate if the energy-dependent lifetime vanishes at the Fermi level depending on the kind of Fermi-liquid. The spectral density is then no longer Lorentzian and is sensitive to the asymptotic law , which can be experimentally investigated. [20, 48] For a peak ϵ'_k within the Fermi sea, Z may be identified with the integral of A^- – compare Eq. (1.55) with (1.59) – which thus corresponds via Eq. (1.53) to the quasi-particle weight of the $T = 0$ occupation number.

In spite of the advantage offered by the quasi-particle picture, there still remains the question whether it is applicable in specific cases. However, if the perturbation theory for the proper self-energy holds and if the self-energy can be analytically expanded in a power series with respect to the perturbation parameter, then quasi-particle states may adequately reflect the excitations provided the obtained lifetime is reasonably long. The latter decreases e.g. in metals with decreasing distance from the Fermi level, so the picture may break down far from it.

For the particular case of photoemission, neglecting the Z factor, the hole GF for a quasi-particle (we should say "quasi-hole") can be written as

$$G(k,\epsilon) = \frac{1}{\epsilon - \epsilon'_k - i\Gamma} \tag{1.60}$$

with $\frac{1}{\hbar}\Gamma = \tau^{-1}$ being the inverse lifetime τ of the single-particle state. This form is particularly useful because it allows us to see a direct connection among GF, spectral function and self-energy, see Eq. (1.21). In fact, if the self-energy can be estimated, all the many body effects can then be described by considering a quasi-particle with renormalized energy equal to $\epsilon'_k = \epsilon_k + \Sigma_r + i\Sigma_i$, where ϵ_k is the energy of the bare particle and the self-energy is

expressed by its real and imaginary parts as $\Sigma = \Sigma_r + i\Sigma_i$. Therefore, we see that the real part of the self-energy describes the correction to the value of the energy of the bare particle, while the imaginary part describes the finite lifetime of the quasi-particle state. In other words, we consider in Eq. (1.60) $\epsilon_k' = \epsilon_k + \Sigma_r$ and $\Gamma = \Sigma_i$.

We thus obtain the following formulas often found in the literature

$$G(k,\epsilon) = \frac{1}{\epsilon - \epsilon_k - \Sigma} = \frac{1}{\epsilon - (\epsilon_k + \Sigma_r) - i\Sigma_i} \tag{1.61}$$

$$A^-(k,-\epsilon) = \frac{1}{\pi}\,\mathrm{Im}\,G(k,\epsilon) = \frac{1}{\pi}\frac{\Sigma_i}{[\epsilon - (\epsilon_k + \Sigma_r)]^2 + \Sigma_i^2} \tag{1.62}$$

1.2.9 Photocurrent

A general expression for the photocurrent in photoemission is given by the expectation value of the current operator, cf. [64], using SI units:

$$\mathbf{j}(\mathbf{r},t) = 2\left(\frac{e\hbar}{2m}(\nabla_{\mathbf{r}}' - \nabla_{\mathbf{r}}) + \frac{ie^2}{m}\mathbf{A}(\mathbf{r},t)\right) G^<(\mathbf{r}t,\mathbf{r}'t)\Big|_{\mathbf{r}'=\mathbf{r}} \tag{1.63}$$

with $G^<$ the *electron-occupation propagator* as denoted by Caroli et al. [17] and $\mathbf{A}$ is the vector potential of the photon field. Imagine replacing the particle operators in $G^<$ by one-particle wavefunctions, then this expression reduces to what one derives for the current in usual quantum mechanics. A gauge is used with vanishing scalar potential. The last term in Eq. (1.63) leads to a paramagnetic contribution proportional to the vector potential $\mathbf{A}$. It occurs as a product of the particle density and $\mathbf{A}$ both taken at the position of the detector which lies far outside the solid, and thus vanishes. One is left with the first part where time has to be made infinite or which has to be averaged over time (according to the Abelian limit) so as to obtain the whole photocurrent, thereby leaving the DC component. The time averaging allows the representation by an energy integral of the Green function by Fourier transformation. However, energy resolution as achieved by experimental analyzers can be theoretically simulated by adding a retarding grid-like artificial vacuum level $W = W_0 + \varepsilon_{\mathrm{kin}}$ at the desired energy far outside the solid. Thus, the energy resolved current at time T with detector at position $\mathbf{R}$ is obtained by differentiating with respect to the work function:

$$\begin{aligned} -\frac{d\mathbf{j}(\mathbf{R},T)}{d\varepsilon_{\mathrm{kin}}} &= -\frac{d}{dW}\mathbf{j}(\mathbf{R},T)\Big|_{W=W_0+\varepsilon_{\mathrm{kin}}} \\ &= -\frac{e\hbar}{m}\frac{d}{dW}(\nabla_{\mathbf{R}'} - \nabla_{\mathbf{R}})G^<(\mathbf{R},\mathbf{R}';T,T)\Big|_{W=W_0+\varepsilon_{\mathrm{kin}}}^{\mathbf{R}'=\mathbf{R}} \end{aligned} \tag{1.64}$$

Here, the Green function includes, besides the full interacting Hamiltonian, an external field which depends explicitly on time. A convenient treatment in the framework of Green-function-based nonlinear transport theory is offered by the *Keldysh technique* [68]. It is very similar to usual ground-state or equilibrium perturbation theory, so the details are not important in this

context. Because the time dependence of the field extends over the total interval of the measuring process, the particle operators in $G^<$ do not only locally depend on the time entering the field. The destruction of a particle at time t_2 occurs when the field could already act upon the ground state for some time. It acts further at times before and after the associated creation of a particle at t_1, resulting in a state whose probability as part of the ground state is probed in $G^<$. These features have to be treated within this kind of perturbation expansion.

The diamagnetic part is expanded in powers of $\mathbf{A}$ according to a perturbation series. The zeroth order of $G^<$ carries no current and the first order contributes to the linear conductivity at the detector, which may be discarded by reasoning similar to the neglect of the paramagnetic current. The first non-trivial part arises in second order, $G^{(2)<}$, showing photoemission as a quadratic response effect. Much higher fields would require orders that are higher than the second considered in the following.

The one-body Hamiltonian of the external field consists of a linear and a quadratic expression in $\mathbf{A}$,

$$h_p + h_d = \frac{ie\hbar}{2m}(\mathbf{A}\cdot\nabla + \nabla\cdot\mathbf{A}) + \frac{e^2}{2m}\mathbf{A}^2 \tag{1.65}$$

a paramagnetic and diamagnetic part, respectively. The latter has to be treated in first order, the former in second order. In the first-order term, the time averaging of the photocurrent appearing in Eq. (1.64) simply yields the time average of $\mathbf{A}^2$ because the field-free ground-state Green functions depend only on the time difference. In frequency space, this means a static field which does not contribute to excitations of non-vanishing energy and thus not to those above the vacuum level for the photocurrent. Only the second order term remains

$$\begin{aligned} &G^{(2)<}(\mathbf{R},\mathbf{R}';T,T) \\ &\quad = \frac{i}{\hbar^2}\int d1\,d2 < N|\psi^\dagger(1)h_p(1)\psi(1)\psi^\dagger(\mathbf{R}',T)\psi(\mathbf{R},T)\psi^\dagger(2)h_p(2)\psi(2)|N> \end{aligned} \tag{1.66}$$

where the notation of space and time variables has been condensed into numbers 1 and 2. The time ordering in this time dependent formalism has already been inserted, thus leading to the above sequence of operators. To lowest order, i.e. no electron-electron interaction contained in the formal time dependence of $\psi^{(\dagger)}(t)$, $G^{(2)<}$ can be decomposed through decoupling into $(\psi,\psi^\dagger)$ pairs (Wick theorem):

$$\begin{aligned} G^{(2)<}(\mathbf{R},\mathbf{R}';T,T) = \frac{1}{8\pi}\int dE \int d^3(r_1,r_2) \\ G^r(\mathbf{R},\mathbf{r}_1;E)h_p(\mathbf{r}_1)G^<(\mathbf{r}_1,\mathbf{r}_2;E-\hbar\omega)h_p(\mathbf{r}_2)G^a(\mathbf{r}_2,\mathbf{R}';E) \end{aligned} \tag{1.67}$$

Here we have abbreviated $h_p(\mathbf{r}) = \frac{ie\hbar}{2m}(\mathbf{A}(\mathbf{r})\cdot\nabla + \nabla\cdot\mathbf{A}(r))$, the retarded $G^r = G - G^<$ and advanced $G^a = G - G^>$ Green functions, and specified the vector potential as $\mathbf{A} = \mathbf{A}(\mathbf{r})\cos(\omega t)$. Expression (1.67) must be inserted into Eq. (1.64) for the photocurrent. Only the absorptive part of $\cos(\omega t)$ contributes, leading to $E - \hbar\omega$. We recall that the above Green functions may still include the whole many-body interaction processes. However, the expansion in the external field cannot be fully decoupled without taking the interaction into

account, i.e. there might be, for instance, a Coulomb interaction taking place between any two electrons before and after the excitation at $\mathbf{r}_1$, which is ignored by decoupling as a product of three Green functions. Instead, one should go back to Eq. (1.66), which consists of a product of six fermion operators to be averaged over the ground state. The presented term corresponds only to that which factorizes into three Green functions which can of course be taken as dressed by the interactions in the form of self-energies. Other terms involve a higher number of Green functions which cannot be accounted for by that dressing. These processes yield an example of vertex renormalization. Let us represent the basic expression of Eq. (1.67) with undressed Green functions by the triangle as in Fig. 1.6a: then possible contributions are represented in Fig. 1.6b, dressing according to Eq. (1.67) as well as renormalizations of the vertex. The Green function considered in the figure has been doubly time-Fourier-transformed into the energy regime.

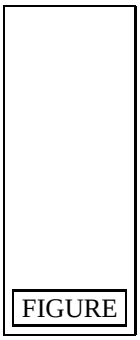

Figure 1.6: Schematic representation of contributions to photocurrent: a) General dressed Green function (top), second order with respect to external field O and interactions neglected (middle), and same as above closed to a vertex with upper corner decorated by external nablas of current (bottom); b) self-energy insertions contributing to the dressing of Green functions in equation (1.67) (top), vertex renormalizations beyond (1.67) (bottom), broken lines represent Coulomb interactions.

The equivalence of Eqs. (1.64) and (1.66) in the one-body limit with the *Golden Rule* formula and with other representations has been shown, see e.g. [31, 74, 75, 96]. With the asymptotics of *outgoing states*, see e.g. [41, 93] (we will come back to that point shortly), we expand with respect to a full set for energies $\varepsilon_k = W_0 + \varepsilon_{\rm kin}$ above the vacuum level W:

$$G^r(\mathbf{R}, \mathbf{r}_1; E) = \sum_k \frac{< \mathbf{R}|\Phi_k^- >< \Phi_k^-|\mathbf{r}_1 >}{E - \varepsilon_k - \mu + i\delta} \tag{1.68}$$

Similarly, G^a is obtained with a negative sign in front of the infinitesimal. Denoting the occupied one-particle bound states by $< \mathbf{r}|j >$ the electron-occupation propagator simplifies to

$$G^<(\mathbf{r}_1, \mathbf{r}_2; E - \hbar\omega) = 2\pi i \sum_j^{occ} < \mathbf{r}_1|j >< j|\mathbf{r}_2 > \delta(E - \hbar\omega + \varepsilon_j - \mu) \tag{1.69}$$

The $\mathbf{R} \to \infty$ behavior of Eq. (1.68) follows from Eq. (1.8) by using the asymptotics of the free-particle Green function which describes an outgoing spherical wave and by expanding in

the exponent $|\mathbf{R}-\mathbf{r}| = R - \mathbf{r}\cdot R/R + ...$

$$G^r(\mathbf{R},\mathbf{r};E) = -\frac{m\sqrt{\nu}}{2\pi\hbar^2 R} e^{ik_0 R} < \Phi^-_{k_0}|\mathbf{r} > \tag{1.70}$$

$$< \Phi^-_{k_0}|\mathbf{r} > = \frac{1}{\sqrt{\nu}}(e^{-i\mathbf{k}_0\cdot r} + \int d^3 r_1 e^{-i\mathbf{k}_0\cdot r_1} V(\mathbf{r}_1) G^r(\mathbf{r}_1,\mathbf{r};E)) \tag{1.71}$$

Periodic boundary conditions with cell volume ν have been applied. The function defined in Eq. (1.70) is the complex conjugate of an asymptotically plane wave with wave vector $\mathbf{k}_0 = \sqrt{\frac{2mE}{\hbar^2}}\mathbf{R}/R$ leading to the detector, accompanied by scattering waves of the potential running into the solid. The function itself shows an "incident" plane wave from the detector to the sample and scattered waves leaving the sample, which characterizes the state in a low energy electron diffraction (LEED) experiment. However, the complex conjugate will appear in the subsequent matrix elements at those positions where the wave function should be present, similar to its appearance in Eq. (1.68). Consequently, it is the time-reversed LEED state which occurs as the final state in photoemission. This result is here inferred from the property of the retarded Green function. Note that $< \mathbf{R}|\Phi^-_{k_0} >$ vanishes below the vacuum barrier, thus a step function $\Theta(E-\mu-W)$ is implicit to the definition of Eq. (1.70).

Quantization of the light as one photon with energy $\hbar\omega$ and unit vector $\mathbf{e}$ of polarization yields:

$$h_p = \sqrt{\frac{e^2\hbar^3}{2\epsilon_0 m^2\omega\nu}}\frac{1}{2}(\mathbf{e}\cdot\nabla + \nabla\cdot e) \tag{1.72}$$

Introducing the matrix elements

$$< \Phi^-_{k_0}|h_p|j > =: \sqrt{\frac{e^2\hbar^3}{2\epsilon_0 m^2\omega\nu}}\Delta_{k_0 j} \tag{1.73}$$

the expression (1.67) becomes:

$$G^{(2)<}(\mathbf{R},\mathbf{R}';T,T) = \frac{im^2\nu}{16\pi^2\hbar^4 RR'} e^{ik_0(R-R')} \int dE \sum_j^{occ} |< \Phi^-_{k_0}|h_p|j >|^2 \delta(E-\hbar\omega+\varepsilon_j-\mu) \tag{1.74}$$

This is inserted into Eq. (1.64) and account is taken of the implicit step function $\Theta(E-W-\mu)$ in $|\Phi^-_k >$ with respect to the lower energy bound at $W+\mu$ when differentiating:

$$-\frac{d\mathbf{j}(\mathbf{R},T)}{d\varepsilon_{\text{kin}}} = \frac{1}{4\pi R^2}\frac{e\hbar\mathbf{k}_0}{m}\frac{e^2}{4\pi\epsilon_0}\frac{1}{\hbar\omega}\sum_j^{occ}|\Delta_{k_0 j}|^2\delta(W_0+\varepsilon_{\text{kin}}+\varepsilon_j-\hbar\omega) \tag{1.75}$$

Equation (1.75) displays the differential photocurrent with respect to kinetic energy $d\varepsilon_{\text{kin}}$ from the flux of one photon. The counts per solid angle $d\frac{d\mathbf{J}}{d\varepsilon_{\text{kin}}}$ are obtained by multiplying

with $R^2 d\Omega$. This is the *Golden Rule* formula, in valence band spectroscopy often denoted as the *one-step model* [91] because it implicitly includes the three steps of excitation, scattering by the lattice and penetration through the surface as a single step. The last two steps are completely contained in the LEED wavefunction whose time reverse obviously enters the matrix elements. The *Golden Rule* condenses these together with the excitation into one coherent process. It is clear that self-energy dressing of the Green functions does not violate the above derivation within the one-particle approximation. Thus, an optical potential in $G^{\,r}(G^a)$ decribes a part of the extrinsic losses that the electron suffers after excitation. Instead of Eq. (1.69) the hole spectral density function A^-, see Eq. (1.52), may be introduced in the position representation, which takes account of intrinsic broadening, as for instance with the finite lifetime of a particle-hole excitation. However, photoelectron-photohole interaction is discarded in both.

The consideration of the general photocurrent is accomplished systematically via the Green function technique described below Eq. (1.67) with an expansion to arbitrary order.

Different physical insight is gained through exact decomposition of Eq. (1.66) with a complete set of states for $(N-1)$ particles, as given by Almbladh's derivation [3]. The time integration is carried out and only the light absorption part is retained, viz.

$$\begin{aligned} G^{(2)<}(\mathbf{R},\mathbf{R}';T,T) = \frac{i}{4}\int d^3(r_1,r_2)\sum_s \\ < N|\psi^\dagger(\mathbf{r}_1)h_p(\mathbf{r}_1)\psi(\mathbf{r}_1)\frac{1}{E_0^N+\hbar\omega-H-i\eta}\psi^\dagger(\mathbf{R}')|N-1,s> \\ < N-1,s|\psi(\mathbf{R})\frac{1}{E_0^N+\hbar\omega-H+i\eta}\psi^\dagger(\mathbf{r}_2)h_p(\mathbf{r}_2)\psi(\mathbf{r}_2)|N> \end{aligned} \tag{1.76}$$

where the index s enumerates the states of the set. The particle operators which appear with their arguments at an asymptotic distance are expanded with respect to a full set of one-particle states, $\psi^\dagger(\mathbf{R}') = \sum_{k'}\phi^\star_{k'}(\mathbf{R}')c^\dagger_{k'}$, chosen to asymptotically exhibit spherical-wave behavior, i.e. $\phi^\star_{k'} \propto \frac{1}{R'}e^{\pm ik'R'}$, both inbound and outbound. We denote as $\varepsilon_{\,k'}$ the corresponding energies of a free particle and consider the first matrix element in Eq. (1.76). An N-particle excited state with an electron at the detector position can be defined as

$$|N-1,s,\mathbf{R}'> \frac{m\sqrt{\nu}}{2\pi\hbar^2 R} := \frac{1}{E_0^N+\hbar\omega-H-i\eta}\psi^\dagger(\mathbf{R}')|N-1,s> \tag{1.77}$$

$$= \sum_{k'}\frac{\phi^\star_{k'}(\mathbf{R}')}{E_0^N+\hbar\omega-E_s^{N-1}-\varepsilon_{k'}-i\eta}(1+\frac{H-E_s^{N-1}-\varepsilon_{k'}}{E_0^N+\hbar\omega-H-i\eta})c^\dagger_{k'}|N-1,s> \tag{1.78}$$

Led by the one-particle derivation above, we consider here the first term in the parentheses which is the only one that remains when $c^\dagger_{k'}|N-1,s>$ is an eigenstate of H with energy $E_s^{N-1}+\varepsilon_{k'}$. Contour integration with respect to $\varepsilon_{\,k'}$ has to proceed along the lower half-plane to yield a non-vanishing result, because it then encloses a pole, located at $\varepsilon_{\,k'} = E_0^N+\hbar\omega-E_s^{N-1}$. Only the negative sign in the exponent of $e^{\pm ik'R'}$ allows closing along the lower half-plane such that only a spherical wave which is incident onto the solid survives. Extracting

this asymptotic factor similar to Eq. (1.70), the sum over the directions $\hat{\mathbf{k}}'$ leaves a state which has to overlap with the emitter volume for non-zero result. This fixes $\hat{\mathbf{k}}' = \mathbf{R}'/R'$ which yields a plane wave incident into the detector with wave vector $\mathbf{k}_0$ because $c^\dagger_{k'}|N-1,s>$ is asymptotically an *outgoing state*, in view of the sign of $-i\eta$. This is characteristic of a time-reversed LEED state, i.e. spherical wave *in* and plane wave *out* as seen from the emitter volume.

The second term in the parentheses corrects for the many-body coupling of this state to the emitter volume. Expanding $\psi(\mathbf{r}) = \sum_j \phi_j(\mathbf{r})c_j$ with respect to a set of states bounded within the emitter volume, inserting in Eq. (1.64), and using $\mu = -W_0$ we arrive at

$$-\frac{d\mathbf{j}(\mathbf{R},T)}{d\varepsilon_{\text{kin}}} = \mathcal{N}\sum_s \Big|\sum_{ij}\Delta_{ij} < N|c_i^\dagger c_j|N-1,s,\mathbf{R}>\Big|^2 \cdot \delta(E_0^N + \hbar\omega - E_s^{N-1} - \varepsilon_{\text{kin}}) \quad (1.79)$$

where $\mathcal{N}$ denotes the normalizing factor in front of the sum in Eq. (1.75). The δ-function of energy conservation arises again via an implicit step function within the state $|N-1,s,\mathbf{R}>$ which must vanish for energies below the detector's vacuum level.

We can see a relation to the sudden approximation by replacing in the notation of $|N-1,s,\mathbf{R}>$ the position $\mathbf{R}$ by the momentum $\mathbf{k}$ of the emitted electron, which is a convenient characterization of the exact outgoing state of Eq. (1.77).

In the *sudden approximation* [50, 51] the photoelectron is approximately decoupled from the solid by defining a particle operator with respect to that state

$$|N-1,s,\mathbf{k}> = c^\dagger_{\mathbf{k}}|N-1,s>$$

with the assumption that $c^\dagger_k$ does not depend on s and vice versa $|N-1,s>$ not on k. It leaves a matrix element $< N|c_i^\dagger c_j c_k^\dagger|N-1,s>$ which couples the isolated photoelectron $c_k^\dagger$ only to the density fluctuation $c_i^\dagger c_j$, but does not influence the choice of the excited $N-1$-particle states $|N-1,s>$. All of the latter are now summed independently disregarding the state of the photoelectron. It is similar to *suddenly* creating the photoelectron in the detector at a probability with which it is contained in the density fluctuations of arbitrary (non-adiabatic) excitations, see also the chapters by Hedin and by Rehr, Albers, and Ankudinov. The property of being sudden becomes still more apparent by approximately equating $c_j c_k^\dagger = \delta_{jk}$, i.e. neglecting its coupling to the fluctuations. The current can then be expressed as

$$-\frac{d\mathbf{j}}{d\varepsilon_{\text{kin}}} = \mathcal{N}\sum_s \Big|\sum_i \Delta_{ik} < N|c_i^\dagger|N-1,s>\Big|^2 \cdot \delta(E_0^N + \hbar\omega - E_s^{N-1} - \varepsilon_{\text{kin}}) \quad (1.80)$$

or with help of the spectral density matrix, see Eq. (1.52),

$$-\frac{d\mathbf{j}}{d\varepsilon_{\text{kin}}} = \mathcal{N}\sum_{ij}\Delta_{ik}A^-_{ij}(\hbar\omega - W_0 - \varepsilon_{\text{kin}})\Delta_{kj} \quad (1.81)$$

Unlike Eq. (1.52), a matrix generalization of the spectral density is implied with analogous definition, namely instead of the same index for both operators c and $c^\dagger$ squared, two indices have been applied. However, in its simplest version this sudden approximation assumes that the hermitean matrix A is already diagonal. With equation (1.81) we are back to the one-particle photoemission formula of Eq. (1.67) inserted in (1.64), with the Green functions appropriately dressed.

At the heart of the sudden approximation lies the assumption that in the photoemission process the photoelectron can be treated as if it were independent from the other particles of the system. Then, the photoemission process can be described as consisting of two decoupled and non interfering processes, the transition from an initial to a final one-particle state of the photoelectron and the many-body response of the $(N-1)$-particle system to the creation of the hole left behind.

The series of approximations within the sudden approximation usually goes further in simplifying the matrix elements Δ_{ik}, in the limit assuming them to be constant. The one-step model whose main achievement was the introduction of the time-reversed LEED state is then entirely lost.

According to their definitions, the spectral functions A^+ and A^- describe the spectrum of the excitation energies when a particle is added or removed from the system and are said to describe the situation of an idealized inverse or direct photoemission experiment. What these approximations omit from a realistic description of photoemission is that the particle will be measured with a detector that is still part of the system, even if separated from the solid by a surface. Also missing is that the process is a result of interaction with light which is associated with a cross section. Last but not least it lacks the treatment of the photoexcited particle with its screened hole when leaving the solid. Thus, in the many cases where the spectral density is taken as the theoretical counterpart of the photocurrent, also called sudden approximation, only a rather poor description is achieved. [39] Nonetheless, since effects of matrix elements and final states on the photoelectron energy distribution are governed by the energy scale of bandstructures, i.e. eV, it may sometimes be possible to single out and identify tiny structures due to many-body interactions on an meV scale, such as those seen in superconducting systems. [19] However, it remains true that the photoelectron is artificially and suddenly decoupled from the many-body system and no interaction is taken into account. Recently, it has been recognized theoretically [6, 78] as well as experimentally [13, 38] that matrix elements and their dependence on the final state are important in high temperature superconductivity and that their neglect could lead to misinterpretations of the spectra.

1.3 Three-step model versus one-step model

By way of introduction to this section, we shall focus on one aspect that has become a long-standing but also increasingly confusing concept, namely the issue of the three-step versus the one-step model of photoemission.

The three-step model dates back to Berglund and Spicer [9] on angle resolved photoemission from solids, which presents a first approach to its theoretical interpretation. The photocurrent is decomposed into three separate factors: the probability of excitation in the bulk solid, the probability of scattering of the excited electron on its path to the surface by

the atoms constituting the solid, and the probability of transmission through the surface for its final acceptance in the detector. The essential point is to calculate separate entities which are easily accessible if they do not interfere with each other. If valence level spectroscopy is the goal, then the focus of attention is on the excitation process from an occupied band state and the photocurrent shows the energy levels at specific directions which are identified with the $\mathbf{k}$ value (i.e. the electron momentum in the bulk). The two remaining factors, scattering and transmission, are considered to be less important: they may even be set to unity by neglecting those effects. By contrast, photoelectron diffraction might lie at the center of interest, as for instance in core level spectroscopy or in imaging methods like holography: in that case, the $\mathbf{k}$ dependence of the occupied states is trivial but the scattering by bulk and surface determines the angle variation of the photocurrent. Then, the first factor, excitation, becomes rather unimportant whereas the other two dominate the interpretation.

In contrast to the three-step model the coherent evaluation of all three steps which *a priori* do interfere is usually denoted as the one-step model. It was originally developed to obtain reliable intensities of valence band spectroscopy for investigating bulk as well as surface characteristics [34], so bringing the accuracy on an equal footing with LEED calculations where refined computer codes existed. [57, 58, 90] Thus, the scattering in the bulk and at the surface is condensed into a coherent final state which must be introduced into the matrix element of photoexcitation, the so-called time-reversed LEED state. [31] As photoelectron-diffraction schemes are closely related to LEED those calculations already obeyed the conditions of the one-step model in principle, though with an important practical simplification by considering only localized, i.e. atomic-like, transitions as they occur in core excitations.

Nowadays, state-of-the-art calculations of photocurrents use the one-step model, even though some valuable short cuts exist. The incorporation of "true" final states which correctly describe the scattering and propagation near and outside a surface is required by the physical situation of accepting the excited electron in the detector at infinite times away from the sample: this is the essential ingredient of the one-step model. The model exists at several levels of sophistication, depending on the extent to which many-body effects are taken into account. Originally, the one-step model was designed as a one-particle theory applying the Golden Rule for one-particle states. The many-body formulation according to the considerations in Section 1.2 in principle should use correct final states as well, and thus fits into the concept of the one-step model. Thus, it would be informative to characterize any given one-step model by describing its level of accuracy in addition to its "one-step" property.

Let us confine the remaining of this section to one single initial state as e.g. in core level spectroscopy. Incorporation of an arbitrary number of states as in the valence band regime will be described in subsequent sections. Current theories of photoemission in solids rely in general on one-electron effective potentials to describe the photoelectron. At low kinetic energies, these potentials must incorporate many-body effects in an effective way (e.g., exchange and correlation via the Hara or other approximation). Then, the photoelectron wave function can be expressed as

$$\psi(\mathbf{r}) = \int d\mathbf{r}' G^r(\mathbf{r}, \mathbf{r}') V_I(\mathbf{r}') \psi_i(\mathbf{r}')$$

where V_I describes the perturbation of the external light, ψ_i is the initial state one-electron

wave function of energy E_i, and

$$G^r(\mathbf{r},\mathbf{r}') = \sum_f \frac{\psi_f^*(\mathbf{r}')\psi_f(\mathbf{r})}{E_i + \hbar\omega - E_f + i\delta}$$

is the Green function of the solid at the photoelectron energy $E_i+\hbar\omega$, cf. Eqs. (1.7) and (1.12). The latter must incorporate all multiple elastic scattering effects of the photoelectron, as well as inelastic processes in which the photoelectron loses energy to create photons, plasmons, or other excitations in the solid.

1.4 Golden Rule

1.4.1 Linear response in the external field

Let us here start with the Hamiltonian of one electron in a system described by a potential $V(\mathbf{r})$, to which an external electromagnetic field is applied:

$$\begin{aligned} H &= \frac{1}{2m}\left(\mathbf{p} - \frac{e}{c}\mathbf{A}(\mathbf{r})\right)^2 + V(\mathbf{r}) \\ &= \frac{p^2}{2m} + V(\mathbf{r}) - \frac{e}{2mc}\left[\mathbf{A}(\mathbf{r})\cdot\mathbf{p} + \mathbf{p}\cdot\mathbf{A}(\mathbf{r})\right] + \frac{e^2}{2mc^2}|\mathbf{A}(\mathbf{r})|^2 , \end{aligned} \tag{1.82}$$

where $\mathbf{A}(\mathbf{r})$ is the vector potential associated with the field. Let us split the Hamiltonian H into two terms ($H = H_0 + V_I$), such that V_I describes the excitation:

$$\begin{aligned} H_0 &= \frac{p^2}{2m} + V(\mathbf{r}) \\ V_I &= \frac{-e}{2mc}\left[\mathbf{A}(\mathbf{r})\cdot\mathbf{p} + \mathbf{p}\cdot\mathbf{A}(\mathbf{r})\right] + \frac{e^2}{2mc^2}|\mathbf{A}(\mathbf{r})|^2 . \end{aligned} \tag{1.83}$$

For low intensities of the external field, first order perturbation theory can be used to study the interaction between the electromagnetic radiation and the system. Thus, applying the Golden Rule to calculate the photocurrent, we obtain:

$$I(f) = |M_{if}|^2 = |<\psi_f|V_I|\psi_i>|^2 , \tag{1.84}$$

where the one-electron wavefunctions ψ_i and ψ_f are eigenfunctions of the Hamiltonian H_0, and the final wavefunction ψ_f behaves as an outgoing wave at infinity (i.e., ψ_f is an inverse LEED state).

The flexibility introduced by the gauge choice in the theory of electrodynamics facilitates the calculation of the matrix element. A common choice is to work in the Coulomb gauge, in which:

$$\nabla\cdot\mathbf{A}(\mathbf{r}) = 0 , \tag{1.85}$$

and consequently

$$(\mathbf{A}(\mathbf{r})\cdot\mathbf{p} - \mathbf{p}\cdot\mathbf{A}(\mathbf{r})) = i\hbar\nabla\cdot\mathbf{A}(\mathbf{r}) = 0 . \tag{1.86}$$

The interaction potential V_I can thus be expressed as:

$$V_I(\mathbf{r}) \;=\; -\;\frac{e}{mc}\,[\mathbf{A}(\mathbf{r})\cdot\mathbf{p}] \;+\; \frac{e^2}{2mc^2}|\mathbf{A}(\mathbf{r})|^2\,. \tag{1.87}$$

So far, the most important approximations introduced in the theoretical formalism are the restriction to a one-electron picture, and the use of only first-order perturbation theory to calculate the interaction between the incident radiation and the system (Eq. (1.84)). The latter approximation is equivalent to neglecting terms of order $\sim |A|^2$ in the calculation of the photocurrent. In order to be consistent with this approximation, the term of order $\sim |A|^2$ in the interaction potential V_I (Eq. (1.87)) is omitted as well. This approximation remains valid provided that the flux of incident photons is relatively low. For higher intensities of the external field these terms cannot be neglected and the theoretical formalism becomes more intrincate.

The matrix element M_{if} after keeping only the lowest-order terms can be written as:

$$\begin{aligned} M_{if} \;=\; <\psi_f|V_I|\psi_i> \;&=\; \frac{-e}{mc}\;<\psi_f|\mathbf{A}(\mathbf{r})\cdot\mathbf{p}|\psi_i> \\ &=\; \frac{ie\hbar}{mc}\;<\psi_f|\mathbf{A}(\mathbf{r})\cdot\nabla|\psi_i>\;, \end{aligned} \tag{1.88}$$

where we have used the identity $\hat{p} = -i\hbar\hat{\nabla}$. This way of writing the matrix element has been usually called in the literature the *velocity form* of the matrix element.

1.4.2 Dipole approximation

The theoretical description of the interaction between the electromagnetic field and the system is usually simplified by means of the so-called *dipole approximation*. The dipole approximation assumes that the variation of the external field $\mathbf{A}(\mathbf{r})$ is small in the spatial region in which the matrix element M_{if} is not negligible. The latter seems a reasonable assumption for the low energy range of the photon spectrum and/or for the photoexcitation of localized electrons, although it is more difficult to justify in some other cases (such as excitation from valence levels). In general terms, it works better in the evaluation of total cross sections than in the calculation of photoelectron angular distributions. Recent measurements in small systems show that significant deviations from the dipole approximation can be found even in systems for which it has been traditionally applied [22]. Nevertheless, let us restrict ourselves to the calculation of the photocurrent in the dipole approximation.

When the external electromagnetic field is periodic in space, it can be expressed as:

$$\mathbf{A}(\mathbf{r}) \;=\; A_0\;\mathbf{e}\;e^{i\mathbf{k}r} \;=\; A_0\;\mathbf{e}\;\left(1 + i\mathbf{k}r + \cdots\right)\,, \tag{1.89}$$

where A_0 is the complex amplitude of the field (a scalar number), $\mathbf{e}$ is a unitary vector in the direction of the light polarization, and $\mathbf{k}$ is a vector pointing in the propagation direction of the field. The dipole approximation consists in keeping only the first term of this expansion in the calculation of the photocurrent via Eq. (1.84) (i.e., it is assumed that $|\mathbf{k}r| << 1$). Notice that the range of $\mathbf{r}$ for which the approximation remains valid is delimited by the spatial extent

of the wavefunctions $\psi_i(\mathbf{r})$ and $\psi_f(\mathbf{r})$. The matrix element in the dipole approximation can thus be expressed as follows:

$$M_{if} \;=\; \frac{ie\hbar}{mc}\, A_0 \;<\psi_f|\mathbf{e}\cdot\nabla|\psi_i> \;. \tag{1.90}$$

Let us remember at this point that the momentum operator $\hat{\mathbf{p}}$ can be written as the commutator of two other operators:

$$\hat{\mathbf{p}} \;=\; -i\hbar\hat{\nabla} \;=\; -\frac{im}{\hbar}\left[\,\hat{\mathbf{r}}\;,\;\hat{H_0}\,\right]\;. \tag{1.91}$$

Hence, if ψ_i and ψ_f are eigenstates of the Hamiltonian H_0, the matrix element M_{if} can be calculated as:

$$M_{if} \;=\; -\frac{ie}{\hbar c}\, A_0\;(E_f - E_i)\;<\psi_f|\mathbf{e}\cdot\mathbf{r}|\psi_i>\;, \tag{1.92}$$

and this is known as the *length form* of the matrix element. A third form, known as the *acceleration form* of the matrix element, is sometimes used in the literature as well:

$$M_{if} \;=\; \frac{-ie\hbar}{mc}\;\frac{A_0}{(E_f - E_i)}\;<\psi_f|\mathbf{e}\cdot(\nabla V)|\psi_i>\;, \tag{1.93}$$

in which the identity

$$\begin{aligned} <\psi_f|\nabla|\psi_i> &= \frac{1}{(E_f - E_i)}\;<\psi_f|\,[H,\nabla]\,|\psi_i> \\ &= -\frac{1}{(E_f - E_i)}\;<\psi_f|\nabla V|\psi_i> \end{aligned} \tag{1.94}$$

has been used.

The three forms of the matrix element are in principle equivalent, provided that ψ_i and ψ_f are eigenstates of the Hamiltonian H_0. This is not always the case in real calculations of the matrix element, and some differences may be found in the final result depending on the form used. See for instance Ref. [81] for a discussion on the most accurate form of the matrix element depending on the problem under study.

For a single atom, the dipole approximation leads to certain selection rules in the symmetry of the photoemitted electron wavefunction. These selection rules can be easily derived by expanding the wavefunctions in the basis set of spherical harmonics $Y_{lm}(\Omega_{\mathbf{r}})$. For the sake of simplicity, let us assume that the initial wavefunction $\psi_i(\mathbf{r})$ of the electron is a core level whose quantum numbers l_i and m_i are well defined. $\psi_i(\mathbf{r})$ thus can be written as:

$$\psi_i(\mathbf{r}) \;=\; R^i_{l_i m_i}(r) Y_{l_i m_i}(\Omega_{\mathbf{r}})\;, \tag{1.95}$$

where $R^i_{l_i m_i}(r)$ is the radial part of the wavefunction.

The final wavefunction after photoemission has a similar form and can be written in general as:

$$\psi_f(\mathbf{r}) \;=\; \sum_{l_f, m_f} R^f_{l_f m_f}(r) Y_{l_f m_f}(\Omega_{\mathbf{r}})\;. \tag{1.96}$$

Let us first take linear polarization of the light, and assume that the polarization $\mathbf{e}$ is parallel to the OZ axis. The incoming light dipole operator (cf. Eq. (1.92)) can thus be expanded as:

$$\mathbf{e}\cdot\mathbf{r} \;=\; \left(\frac{4\pi}{3}\right)^{1/2} r\, Y_{10}(\Omega_{\mathbf{r}})\;. \tag{1.97}$$

The expansions of the wavefunctions and the dipole operator can be introduced into Eq. (1.92) to obtain the matrix element as:

$$\begin{aligned} M_{if} \;=\; & -\frac{ie}{\hbar c}\,A_0\,(E_f-E_i)\left(\frac{4\pi}{3}\right)^{1/2}\sum_{l_f,m_f}\left\{\int \mathrm{d}r\; r^3\left[R^f_{l_f m_f}(r)\right]^*\,R^i_{l_i m_i}(r)\right\} \\ & \times\;\left\{\int d\Omega_{\mathbf{r}} Y^*_{l_f m_f}(\Omega_{\mathbf{r}})Y_{10}(\Omega_{\mathbf{r}})Y_{l_i m_i}(\Omega_{\mathbf{r}})\right\}\;. \end{aligned} \tag{1.98}$$

The integral over angles $\Omega_{\mathbf{r}}$ determines the allowed symmetries for the final states. According to general properties of the spherical harmonics, this integral is different from zero only if $l_f = l_i \pm 1$ and $m_f = m_i$.

If the incoming light is circularly polarized, the mathematical description can be also simplified by modifying the geometry. In this case, let us take the OZ axis as parallel to the direction of propagation of the light. Hence the plane of polarization of the light is perpendicular to the OZ axis, and the incoming light dipole operator can be written as:

$$\mathbf{e}\cdot\mathbf{r} \;=\; \left(\frac{8\pi}{3}\right)^{1/2} r\, Y_{1m}(\Omega_{\mathbf{r}})\;, \tag{1.99}$$

where $m = 1$ corresponds to *right* circularly polarized light and $m = -1$ corresponds to *left* circularly polarized light (although the opposite convention is sometimes found in the literature as well). The matrix element for circularly polarized light can be calculated in a similar way as the matrix element for linear polarization (Eq. (1.98)). We only need to replace the spherical harmonic $Y_{10}(\Omega_{\mathbf{r}})$ by $Y_{1m}(\Omega_{\mathbf{r}})$. As a consequence, the integral over angles $\Omega_{\mathbf{r}}$ now generates new selection rules: $l_f = l_i \pm 1$ (as before), but $m_f = m_i + m = m_i \pm 1$.

The selection rules in the dipole approximation are strictly valid only for atomic systems. Nevertheless, in the case of molecules, clusters or solids, the scattering theory provides a simplified picture in which the selection rules fit as well. The photoemission process from a core level can be described as the photoexcitation from a single atom, followed by the transport of the photoelectron on its way to the detector. In this picture, the selection rules remain valid for the first step of the process (the photoexcitation from the single atom). The subsequent scattering of the outgoing electron by the surrounding atoms will add other partial-wave contributions to the final photoelectron pattern.

1.5 Initial state

1.5.1 Core levels

In core level spectroscopy photoelectrons emerge from single atomic levels which simplify the initial state as far as the single particle picture is concerned. Chemical shifts may change the

levels due to local effects near a surface, but the levels may still be considered to be independent (not counting systematic atomic-like degeneracies). Therefore, we will discuss this topic within the description of the final states, see Section 1.6, where the core level emission constitutes the simplest case to be treated. A rather more complicated situation arises if many-body effects are considered, see e.g. [87]. Then, the relaxation of the core hole multiplet together with its interaction with the photoelectron represents a challenging problem. Progress in this field is described in chapter [49] of this handbook. Aside from spectroscopy, in an extremely important development core level emission has served as source for photoelectron diffraction and holography [27] (see chapter [47] and chapter [28]), owing to the localized nature of the source of emission.

1.5.2 Valence bands

Angle resolved photoelectron spectroscopy represents the most general tool for full valence band investigation at highest accuracy. The aim is to extract from the photocurrent the bandstructure over the whole Brillouin zone. Though *ab initio* bandstructure calculations have reached a high level of reliability, their accuracy is limited by computational restrictions and the physical border line of many-body effects. Thus, the experiment is needed as confirmation on one hand and as access to uncover new properties not considered in the bandstructure calculation on the other.

The interpretation of valence band spectra uses intuitive methods relying more or less on energy and momentum conservation or is assisted by full calculations of the intensities, at best. To discuss both, we write the Golden Rule formulation taking into account the continuum of valence band states ψ indexed by the band ν and the three-dimensional momentum $\mathbf{k}$

$$I \propto \sum_{\nu\mathbf{k}} \; | < \Phi^{\star}_{LEED}(E, \mathbf{k}^{0}_{\parallel}) \mid \mathbf{O} \mid \psi_{\nu}(\mathbf{k}) > |^{2} \delta(E - E_{\nu}(\mathbf{k}) - \hbar\omega). \qquad (1.100)$$

The final state Φ depends on the surface parallel momentum $\mathbf{k}^{0}_{\parallel}$ and on the final state energy E which corresponds to the perpendicular momentum component in vacuum. The index LEED relates to a LEED state and the star refers to its time inverse. Energy conservation is guaranteed by the δ-function. Momentum conservation is reduced to the parallel momentum. It arises from the evaluation of the matrix element with operator $\mathbf{O} = \mathbf{A} \cdot \mathbf{p} + \mathbf{p} \cdot \mathbf{A}$. Translational invariance is only maintained parallel to the surface, the vector potential being assumed constant in the case of long wavelengths, including the vacuum ultraviolet regime. Discrete translations according to the lattice periodicity are meant here when speaking about invariance and the Bloch vector is thus associated with momentum. The surface breaks invariance in the perpendicular direction. The parallel momentum which is calculated in vacuum through kinetic energy and direction of the detector has to be folded back into the first surface Brillouin zone to be identified with $\mathbf{k}^{0}_{\parallel}$ of Eq. (1.100).

From Eq. (1.100) it is obvious that three-dimensional momentum will be conserved if one replaces the final state by any eigenstate of a system with three-dimensional translational invariance. This is done within the *band-mapping* scheme where in the simplest case the final states are taken to be three-dimensional plane waves. In a more sophisticated treatment, the set of eigenstates of the bulk may be used as final states. Furthermore, solving the bulk hamiltonian with complex Bloch vectors generalizes this set and admits exponentially decreasing and increasing solutions; of the latter only those which increase in the direction towards the

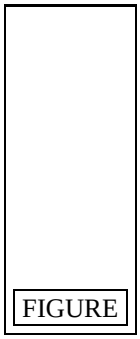

Figure 1.7: Ab initio computed spectrum of GaAs(001) for photon energy 28 eV (lower part) deconvoluted to yield peaks at energies marked by bars with full dots, compared with bare bars mapped from intersections of initial bands (black lines) with final bands (flat curves) shifted by photon energy down to binding energy scale (upper part), one example shown by dotted line; insert shows density of states and a matrix element, position of direct transition near -4.5 eV indicated.

surface are physically reasonable. All these sets are eigenstates of the Bloch momentum and thus conserve the total momentum in the matrix element. The interpretation of the photocurrent within these schemes identifies the possibilities of transitions between all valence states and all final states belonging to the chosen set and allowed by energy and three-dimensional momentum conservation, the so-called *direct transitions*. Primarily, this takes advantage only of the spectral peak positions. Their height will correspond in some way to the weight of the matrix element and their width may be associated with the lifetime of the valence states. In any case, this description yields a mapping between momentum and energy for all momentum space points which can be associated with peaks in the spectra, i.e. it yields parts of the bandstructure. [32, 65] It is more or less accurate depending on the ability to define a clear peak.

The accuracy of the band-mapping can be estimated by comparing it with a full calculation of Eq. (1.100). In Fig. 1.7 a spectrum computed accordingly is presented and interpreted by direct transitions which is represented by bars on top of the peaks obtained by a deconvolution procedure. Any of the known deconvolution techniques leads to similar positions. Above the spectrum the valence bandstructure together with the complex bandstructure is shown shifted by the amount of the photon energy such that the intersections give the allowed direct transitions. These intersections are also marked by bars in the spectrum. If both kinds of bars agree in position the momentum associated with the intersection has to be attributed to the peak and its binding energy. Of course, only distinct peaks may be considered. However, the result of Fig. 1.7 shows clear misfits which reach up to 200 meV. If we had taken the peaks of the spectra to be granted and with a knowledge of the final states bandstructure, had extrapolated through their energy to the associated momenta, then the momentum would be wrong and the maximum error in energy could reach values up to 200 meV. This error is large compared to the actual energetic resolution of photoelectron spectroscopy which can be below 10 meV. Nevertheless, it is the most advanced procedure within the framework of band-mapping, using the complex bandstructure, i.e. eigenstates of a hamiltonian which simulates

the solid-vacuum system by bulk.

A different but less instructive view on the observed spectra entirely neglects the final states' bandstructure: it assumes that, because of the dense distribution of excited states at high energies, the δ-function can always be fulfilled and the matrix elements are constant throughout. Then the sum over initial states in Eq. (1.100) condenses into the density of initial states. As the parallel momentum is prescribed by the detector, this is a one-dimensional density of states which counts the states per energy only along the perpendicular direction. The selection rule for the perpendicular momentum is replaced now by the dominance of band edges and critical points, the only structures in the spectra surviving in this model. A single direct transition would have no weight, e.g. see insert of Fig. 1.7.

In physical reality both pictures, band-mapping and density of states, will contribute. However, the amount of nonconservation of perpendicular momentum and the necessity to refer to density-of-states effects can be estimated with a knowledge of the final states' bands. The final state in Eq. (1.100) can be decomposed in the interior of the solid with respect to the complex Bloch vector states and a weight is associated with each. The imaginary part of the Bloch vector partly results from the imaginary part of the self-energy and partly from the damped penetration from surface into bulk if the electron's energy coincides with a forbidden gap region. It determines the momentum broadening of the surface perpendicular component and thus limits the admissable uncertainty for a deviation. The equation sums up all these contributions. Other transitions cannot occur and thus the density-of-states effect has to be embedded in direct transitions.

In contrast with its general deficiencies, the density of states interpretation has experienced a development towards many-body effects. The energy conservation δ-function can be seen as the imaginary part of the Green function if the imaginary part of the self-energy tends to zero. For finite lifetime this becomes the spectral density in the framework of many-body theory. The δ-function including valence wavefunction and the sum over band index ν has to be replaced by the spectral density matrix $A^{-}_{ij}(\mathbf{k}, E)$ in the representation by any basis set $\mid i >$ with fixed Bloch vector $\mathbf{k}$ via

$$\sum_{\nu} \delta(E - E_{\nu}(\mathbf{k})) < i \mid \psi_{\nu}(\mathbf{k}) >< \psi_{\nu}(\mathbf{k}) \mid j > \rightarrow A^{-}_{ij}(\mathbf{k}, E), \tag{1.101}$$

see equation 1.52 where index k now denotes $(\nu, \mathbf{k})$. Thus, it takes into account the correct many-body distribution of valence levels if the terms with the Dirac brackets are generalized to the many-body transition amplitudes $< \Psi_n^{N-1} | \widehat{c}_i(\mathbf{k}) | \Psi_0^N >$ of Green functions in Eq. (1.101):

$$I \propto \sum_{ij\mathbf{k}} < \Phi^{\star}_{LEED}(E, \mathbf{k}^{\mathbf{0}}_{\parallel}) \mid \mathbf{O} \mid i >< j \mid \mathbf{O}^{+} \mid \Phi^{\star}_{LEED}(E, \mathbf{k}^{\mathbf{0}}_{\parallel}) > A^{-}_{ij}(\mathbf{k}, E) \tag{1.102}$$

compare with equation 1.81 and the discussion following it. In practice, one neglects the whole non-valence part of the Golden Rule, i.e. final states as well as matrix elements, and takes merely the diagonal A to represent the photocurrent. This procedure may be justified for instance in cases where the interesting structures of the photoemission spectra vary rapidly as compared to the variation induced by matrix elements. The latter is characterized by band energies of the order of magnitude of eV. As a consequence, the analysis of spectral features from HTC superconductivity with a meV scale of variation may be justified. [82]

Between the direct transition and density of states interpretations a series of intermediate schemes have been proposed in the literature, some of them occurring also in the context of other chapters in this book, where they are further described.

In the following, we present specific examples of full one-particle calculations in the framework of the Golden Rule formula.

The first main development in this respect concerned photoemission from metals for which the use of muffin-tin potentials in the framework of a multiple scattering method is suitable. [57, 91] The layer-KKR code had the time inverse LEED state implemented according to the calculational schemes for LEED intensities and used KKR for the valence state as well. It was thus designed for surfaces. Eq. (1.100) written in position space with help of the hole Green function G^{hole} reads

$$I \propto \mathrm{Im} \int d^3r \int d^3r' < \Phi^{\star}_{LD}(E, \mathbf{k}^{\mathbf{0}}_{\parallel}) \mid \mathbf{O} \mid \mathbf{r} > G^{hole}(\mathbf{r}, \mathbf{r}', E - \hbar\omega, \mathbf{k}^{\mathbf{0}}_{\parallel}) \qquad (1.103)$$
$$\cdot < \mathbf{r}' \mid \mathbf{O}^{+} \mid \Phi^{\star}_{LD}(E, \mathbf{k}^{\mathbf{0}}_{\parallel}) >$$

Both the Green function and the LEED state are expanded in terms of spherical harmonics in order to use the KKR scheme. An important simplification arose from the use of the matrix element in the acceleration form because between the muffin-tin spheres the potential V is constant. The integration in the matrix element is thus confined within the muffin-tin spheres: the wavefunctions need to be constructed here. An obstacle in this muffin-tin scheme was found in the treatment of the potential barrier at the surface.

This method has been further completed by generalizing to the relativistic case [1,2,14,15, 40,46,105] The 2x2 spin density matrix $\rho_{\tau,\tau'}$ is evaluated via a formula similar to Eq. (1.103) where the four component Dirac spinors $< \Phi \mid$ and $\mid \Phi >$ carry the index τ and τ', resp., $G^{<}(\mathbf{r}, \mathbf{r}')$ is a 4x4 component Dirac matrix, and the transition operator $\mathbf{O}$ contains the vector potential as $\alpha \cdot \mathbf{A}$ using 4x4 matrices $\alpha_{ik} = \sigma(1 - \delta_{ik}), i, k = 1, 2$ with Pauli spin matrices σ. Spin-averaged photocurrent, spin polarization, and individual spin-resolved photocurrent are obtained via spin averaging of the respective observables with the spin density matrix. A transformation analogous to Eq. (1.93) confining integration to the muffin-tin spheres can be used in this case, too.

The above scheme was further developed to include non-spherical parts of the potential. [44] The multiple scattering scheme remained essentially the same. However, instead of a muffin-tin model the Wigner-Seitz cell with the so-called "true potential" inside and zero outside the cell was taken to solve the Schrödinger equation within the circumscribing sphere and matching to free solutions outside. The result served as the basis for the multiple scattering expansion.

The LEED scheme and similarly the above approaches according to their initial design showed slow convergence for low kinetic energies with low damping. Additionally, the full potential yields non-diagonal t-matrices which slows down the code again. A limitation to spherical potentials was out of the question when considering semiconductors. Especially, surface reconstructions specific to semiconductors made the scheme rather cumbersome. The surface bandstructure could not be obtained within the Bloch scheme used leading to the complex bandstructure only. The photoemission part of the code met similar difficulties in treating emission from surface states which near the valence band maximum are scarcely damped.

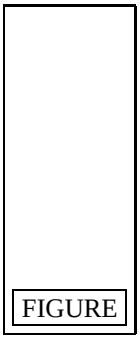

Figure 1.8: Theoretical and experimental pattern of photocurrent into emission hemisphere with $h\nu = 26$ eV from Fermi energy for $TiTe_2(0001)$ (bottom); Fermi surface plot (top left) compared with energy surface slightly above E_F (top right) .

Thus, a separate approach was developed for such materials. It benefits from the existence of self-consistent ab-initio calculations for the bandstructure. A suitable basis $\mid \psi_i >$ adapted to or directly taking those solutions forms the representation for the initial states. It is condensed in a Green matrix G_{ij} for the halfspace system which includes an arbitrary surface potential and is used in Eq. (1.100) to yield

$$I \propto \mathrm{Im} \sum_{i,j} < \Phi^{\star}_{LD}(E, \mathbf{k}^{\mathbf{0}}_{\parallel}) \mid \mathbf{O} \mid \psi_i > G^{<}_{ij}(E - \hbar\omega, \mathbf{k}^{\mathbf{0}}_{\parallel}) \cdot < \psi_j \mid \mathbf{O} \mid \Phi^{\star}_{LD}(E, \mathbf{k}^{\mathbf{0}}_{\parallel}) > \tag{1.104}$$

The basis normally chosen used a layer resolved LCAO set with Bloch sums along surface parallel layers and respective Bloch vectors $\mathbf{k}^{\mathbf{0}}_{\parallel}$. Ab initio pseudopotentials are used for the evaluation of final states.

As an example, the result of a calculation via 1.104 for $TiTe_2$ is presented in Fig. 1.8. Slight deviations in binding energy shown by the different energy surfaces in that figure can be discriminated by a comparison of experimental with theoretical photoemission patterns which confirms the matching of both energy scales in this case. The demand of computer ressources for such a calculation consists of the whole of separate runs for each angle and sums up to a still considerable amount even within this code which is fast compared to the original KKR schemes.

1.6 Final state

We now turn our attention to the final state. This higher-energy state describes how the photoelectrons scatter and propagate as they leave the emitter site and travel to the detector in the vacuum outside the solid.

One point to keep in mind is that an electron in the final state senses a different potential than an electron in the initial state: the difference in kinetic energy causes differences in the effective potential felt by an electron.

1.6.1 Direct solution of Schrödinger equation

In contrast to the multiple scattering procedure which actually uses Green functions as to be subsequently discussed, the final states of photoemission may be directly incorporated via their wavefunctions. This is especially useful in the low kinetic energy range where the anisotropic potential in the interstitial region and at the surface becomes important. Plane-wave based descriptions are convenient in a pseudopotential version though augmented plane waves have started to be applied, too. [70] Thus, the path to an all-electron computation is paved. The pseudopotential formalism is comparably fast and has been applied in most cases.

The evaluation of wavefunctions proceeds via a direct solution of the Schrödinger equation. The formulation of the boundary condition is a little tricky because physical intuition would view it as an initial value problem solved backwards in time. The photoemission final state in principle must be described as an outgoing state with plane wave asymptotics characterized by the observed momentum in the detector at infinite time. Time is replaced by the coordinate perpendicular to the surface such that plane wave asymptotics are required at infinite distance from the surface in vacuum. An elliptic equation encounters numerical instabilities which become apparent when using a step procedure as solver. One has to transform the asymptotic condition into a boundary condition for a closed domain. This can be done at a sufficiently remote interface within vacuum which leads to mixed boundary values, i.e. a relation between the function and its derivative at that interface. [79] In formulating these conditions use has been made of smooth continuity and vanishing potential at that fictitious interface. It might be interesting to note that on the vacuum side of that interface a single plane wave travels to the detector whereas a set of plane waves propagates towards the interface in order to satisfy a correct matching. From the solid side a similar set is impinging onto the surface such that the time reverse of all the terms constitutes a so-called scattering solution, i.e. one plane wave incident and scattered waves into all directions. This degenerates here, because of the unboundedness of the laterally infinite scatterer, into two sets of scattered waves travelling away from the interface into both half-spaces.

An intermediate step deserves separate consideration because it is appropriate for a shortcut interpretation of photoemission data. One obtains the complex bandstructure as the solution of the inverse bandstructure problem, i.e. prescribing the energy and solving for the eigenvalues of the perpendicular momentum. The Bloch condition yields real and complex values for that momentum, which is obvious especially for energies within the gap. One set, that with exponentially increasing wavefunctions towards the semi-infinite bulk, is discarded, but the remaining set constitutes a full set of states which are bounded in the bulk and are bounded up to the surface in the opposite direction. The energy vs. Real($k_\perp$) relation yields the complex bands with their imaginary part describing the exponential drop-off of such a band state in the interior. Considering the correct solution as a superposition of such states, those with large imaginary part will contribute less in view of a matching at the surface to the outside solution. The spatial variation proceeds on a scale given by the kinetic energy and this yields an order of magnitude beyond which a significantly shorter scale of decay will not contribute. Plotting the complex bandstructure for only reasonably low imaginary part together with the real bandstructure of the initial states of photoemission gives a first impression of the photocurrent to be expected in the direct transition model. Figure 1.9 shows electron distribution curves (EDC) for normal emission for GaN in comparing theory with experiment. [23]

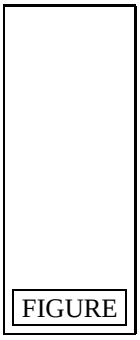

Figure 1.9: Theoretical (middle) and experimental [23] (right) normal emission spectra from Ga terminated GaN(0001)1x1, intensity vs. binding energy for various photon energies as marked, with single spectrum (bottom left) and both initial and complex final bandstructures (top left) for photon energy 35 eV; vertical bars at theoretical spectra indicate main direct transitions; final state decomposes into complex bands with weights denoted by bars at curves; both band systems are brought to coincidence through shifting by photon energy.

Agreement is obtained that is typical for this spectroscopy. The origin of the theoretical peaks is traced back in that figure to the intersection of the initial bands, shifted by the photon energy, with the final bands thereby assuming direct transitions, i.e. strict momentum conservation. The dispersion of the peaks with photon energy is indicated by dotted lines as a guide to the eye. Following the binding energies of the intersections when the bandstructures' shift by the photon energy is varied scans the observed dispersion in the theoretical and experimental spectra. In many cases it is appropriate to relax the accuracy slightly and to simplify the system so that it consists of the bulk pseudopotential including an optical potential and the sharp edge of a step-potential. In examples which need a more accurate modelling, e.g. of a surface layer, two potential steps are convenient as well. Then, a simple matching of the wavefunctions, i.e. plane waves in the region of constant potential and Bloch states of complex bandstructure in the bulk, gives reasonable results if used for the final states of a one-potential-step calculation. Matching instabilities at single energies occur which are manually removed by considering energies close by. This difficulty and the lack of some accuracy is balanced by an appreciable gain in computational time. The spectra in Fig. 1.9 are calculated by this scheme with one potential step.

Among several methods for the practical solution of the above mentioned boundary value problem, using the Laue representation together with layer doubling proved to be the fastest. The basis of that representation consists of plane waves in the surface parallel directions, their coefficients depending on the perpendicular coordinate z. The latter solve a system of ordinary differential equations (indexed by the reciprocal lattice vectors of the plane waves) with suitable boundary conditions with respect to the perpendicular coordinate. Discretizing z leads to an algebraic system with a matrix that is band diagonal with respect to z in its kinetic energy part but also in its potential part, provided the latter has a suitably limited range. With respect to the discretized z a layer doubling renormalization converges rapidly to the entire halfspace. The method uses pseudopotentials. Ab-initio pseudopotentials have to be transformed to a quasi-local form. [5, 11, 98] An example for such a final state wave function

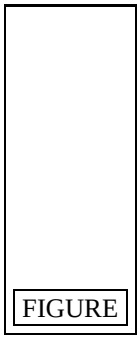

Figure 1.10: Plot of phase, a and d, and modulus, b and c, of wavefunction for Si(001) entering surface from vacuum (top) to solid (bottom), inclied electron escape (a,b), normal escape (c,d); dots show nuclei positions, frame indicates interface.

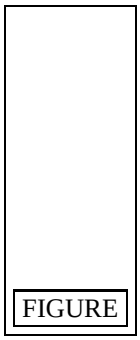

Figure 1.11: Wave functions Fourier transformed along (0001) direction ($A\Gamma A$) of $TiTe_2$(0001), for each energy intensity of shading represents modulus of Fourier coefficient vs. wave vector; real band-structure (black lines)is underlaid.

is shown in Fig. 1.10. Phase coherence is quickly lost in penetrating into the solid via more inclined directions. The potential may contain complex parts to account for the optical potential or more general many-body corrections, see below. In an example for $TiTe_2$ a series of final state wave functions between 5-100 eV has been computed and subsequently Fourier transformed with respect to its surface perpendicular position dependence to yield Fig. 1.11. Only slight differences occur by either fixing somehow or averaging the surface parallel position component. It is an obvious message that only one band, which, of course, is backfolded and actually is close to a parabola, dominantly contributes, i.e. plane waves distributed in a rather narrow range around the the parabolic dispersion constitute mainly the final state. This is often anticipated in experimental analyses. It was found for the layered transition metal dichalcogenides and for III-V semiconductors. However, the distribution becomes broader for higher energies and furthermore, the behaviour is best established for normal emission and deteriorates for inclined directions. The experimental confirmation of the correctness of the final states' calculation arises from ARUPS rather indirectly because the latter is primarily determined by the initial states in valence band spectroscopy. Core-level initial states might

give a more direct access because of their lack of dispersion, but that is not yet in actual favor. A direct method is available via very low energy electron diffraction (VLEED) with intensity spectra, $I(U)$, which yield the angle dependent electron reflection and absorption in the elastic channel. This is intimately described by the wavefunctions used for the final states which can thus be tested. [104]. Total current spectroscopy represents the complementary case of this method. [89, 98] A simple illustration follows from the fact that the incident electron is strongly reflected by the surface in those energy regions where a gap appears in the bandstructure of the solid.

Finally, the obtained wavefunction is inserted into the Golden Rule, Eq. (1.100), for $|\Phi^{\star}_{LD}(E, \mathbf{k}^{\mathbf{0}}_{\|}) >$ which is integrated in direct space to calculate the photocurrent.

At this point, a remark must be made about the optical potential physically motivated by the losses of the propagating electron and a necessary ingredient for convergence in the bulk. Seen from many-body theory, such losses are represented by the lifetime of a quasi-particle state, which corresponds to the imaginary part of the self-energy Σ. Apart from heuristic approaches to this quantity, especially to its energy dependence, it can be calculated nowadays in a more systematic way, e.g. via the "GW" approximation, i.e. writing the self-energy as a product of the Green function G and the screened Coulomb interaction W according to the first term of an expansion with respect to W. Then the real part of Σ is accessible, too, and the entire quantity may be used as the quasi-particle correction to the final state. The solution for these states as described above can include the self-energy in a very general form, i.e. more general than in a merely energy dependent form.

The presence of the self-energy is required within the quasi-particle Green function which in turn is obtained by Dyson's equation, on one hand. On the other hand, the self-energy is represented by a set of quasi-particle states which are obtained from a solution of the homogeneous variant of the Dyson equation which corresponds to the usual Schrödinger equation plus a complex Σ. Thus, in the excited energy regime these states may be considered as final states of photoemission taking suitable boundary conditions. [98] In the occupied energy regime they represent the initial states. It follows that, because Σ is energy dependent, both sets of states belong to different one-particle hamiltonians even for the hermitean no-loss case. Therefore, it is not required that the states emerge from one single hamiltonian. This gives freedom to treat the states by different methods adapted more specifically to each energy range.

The form of $\mathrm{Im}\,\Sigma$ in the final states' regime follows a general shape, specifically, it increases from a low value, below a tenth of an eV at the bottom of the conduction states, with a significant jump at the plasma frequency up to several eV in the VUV range of photoelectron spectroscopy. The increase through plasmon losses is sometimes modelled by a Fermi function-like shape. [43] The consequence of that increase is generally an increase of the imaginary part of the Bloch vector and consequently of the perpendicular momentum non-conservation or spread of indirect transitions. It does not increase the width of the photoemission peaks. That is determined by the lifetime of the occupied states. Actual state-of-the-art calculations use the GW approximation. [35, 37, 97] A comparison for $TiTe_2$ between the heuristic shape and that calculated by GW for the unoccupied states reveals a rough agreement in the overall dependence whereas the details differ, see Fig. 1.12. Slope and edge position can thus be calculated. The asymptotic decrease in the magnitude of the GW result is attributed to the energy cut-off.

Some additional structure is present in the GW plot and is reminiscent of the electronic

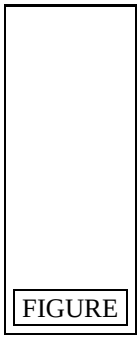

Figure 1.12: $\mathrm{Im}\,\Sigma$ as matrix in reciprocal lattice vectors calculated with GW for diagonal elements (left), (1,1) element to be compared with empirical optical potential, and for non-diagonal elements (right).

transitions which appear in the dielectric function involved in the screened interaction W. However, the details are smoothed by the integrations involved in the calculation. A scheme for an independent determination of ($\mathrm{Im}\,\Sigma$) via VLEED has been recently described. [72]

1.6.2 Multiple scattering method

An alternative approach for dealing with the final state wave function is to actually consider the individual scattering events suffered by the photoelectron in its elastic interaction with the solid atoms along its way to the detector. This is the so called multiple scattering (MS) method, which consists in calculating the one-electron wave function of the photoelectron as the sum of the direct unscattered photoemission wave and the result of MS due to the surface atoms.

In this context, the surface atoms are usually described by spherically-symmetric muffin-tin potentials, and this is a good approximation for electrons with relatively high kinetic energy ($E > 50$ eV); these are insensitive to the details of the atomic potential tails and see the atoms basically as spherical entities [90]. The generalization to space-filling arbitrary potentials can be made with some care [42].

Two basic approaches are in use to represent a surface: the semi-infinite model which preserves periodicity in two dimensions, and often truncates the surface to a finite depth as a slab; and the cluster model, which retains only a finite-size piece of the surface, thus more easily allowing non-periodic structures to be represented. The semi-infinite model is used in particular in the work of Pendry, Tong and others [91, 107] In the following, we will describe the cluster model, which is simpler but also functions as an ingredient in many semi-infinite models.

Thus, we shall approximate the solid by a cluster of non-overlapping spherical muffin-tin potentials. The size of the cluster is dictated by the finite electron mean free path. Each muffin-tin potential represents a solid atom centered at a position $\mathbf{R}_\alpha$. The potential outside the muffin-tin spheres and within the solid is set to a constant value, the muffin-tin zero, to which the photoelectron energy E is referred. The effect of inelastic attenuation is incorporated by

adding a small imaginary part to E [90] (which is equivalent to adding it to the photoelectron self-energy).

For simplicity, we shall consider core-level photoemission, so that the initial-state wave function is fully contained within the muffin-tin sphere of the emitter atom, which we will denote α_0. This will be generalized to extended initial states (e.g., in valence photoemission) in Sec. 1.7.

To represent scattering by the atoms, the electron wave function is then expressed in spherical harmonics and spherical Bessel functions centered on each atom of the cluster. In particular, the direct photoelectron wave function ϕ^0 (that is, the wave which originates at the emitter in the absence of MS) can be projected on a complete basis set of outgoing and incoming spherical waves centered on the emitter, and the physical requirement that there should be no net incoming flux for any partial wave component leads to the fact that only outgoing waves contribute in this case. More precisely,

$$\phi^0(\mathbf{r}) = \sum_{L'} h^{(+)}_{L'}[k(\mathbf{r} - \mathbf{R}_{\alpha_0})]\, \varphi^0_{L'} \tag{1.105}$$

for $\mathbf{r}$ outside the muffin-tin sphere of the emitter α_0, where $h^{(+)}_L(k\mathbf{r}) = \mathrm{i}^l h^{(+)}_l(kr) Y_L(\Omega_{\mathbf{r}})$ represents an outgoing spherical wave, $h^{(+)}_l$ is a spherical Hankel function [85], $L = (l, m)$ labels spherical harmonics Y_L, and $k = \sqrt{2E}$ is the electron momentum relative to the muffin-tin zero.

In order to study MS effects, we need to consider $\phi^0(\mathbf{r})$ near the other cluster atoms $\alpha \neq \alpha_0$. This can be conveniently done by expressing each of the partial waves L' of ϕ^0 in terms of spherical waves centered on another atom $\alpha \neq \alpha_0$, which can be done by using the translation formula of spherical harmonics [88]

$$h^{(+)}_{L'}[k(\mathbf{r} - \mathbf{R}_{\alpha_0})] = \sum_L j_L[k(\mathbf{r} - \mathbf{R}_\alpha)] G_{\alpha\alpha_0,LL'}, \tag{1.106}$$

where

$$\begin{aligned} G_{\alpha\alpha_0,LL'} = 4\pi \sum_{L''} & h^{(+)}_{L''}[k(\mathbf{R}_\alpha - \mathbf{R}_{\alpha_0})] \\ & \times \int d\Omega\, Y_L(\Omega) Y_{L''}(\Omega) Y^*_{L'}(\Omega) \end{aligned} \tag{1.107}$$

and $j_L = \mathrm{i}^l j_l Y_L$ is a spherical wave centered at α that can be regarded as the spherical component of a plane wave passing by atom α.

The above translation allows one to express Eq. (1.105) as a sum of j_L waves in the vicinity of a given atom α. The contribution of the scattering of these waves from α is obtained if we make the substitution

$$j_L \to j_L + \sum_{L'} t_{\alpha,L'L} h^{(+)}_{L'}, \tag{1.108}$$

where $t_{\alpha,LL'}$ is the so-called scattering matrix, which for spherical atoms, becomes diagonal and is given in terms of the scattering phase shifts δ^α_l as [85]

$$t_{\alpha,LL'} = t_{\alpha,l}\delta_{LL'} = \sin\delta^\alpha_l \mathrm{e}^{\mathrm{i}\delta^\alpha_l}\, \delta_{LL'}. \tag{1.109}$$

The second term in Eq. (1.108) is the scattered part of a plane wave component, as obtained by standard partial wave analysis [90]. Then, summing over all possible first-order scattering events (i.e., over all atoms α), the photoelectron wave function calculated within first order reduces to

$$\phi^1(\mathbf{r}) = \sum_{\alpha} \sum_{L'} h_{L'}^{(+)}[k(\mathbf{r} - \mathbf{R}_\alpha)]\, \phi^1_{\alpha,L'}, \tag{1.110}$$

where

$$\phi^1_{\alpha,L'} = \phi^0_{\alpha,L'} + \sum_{LL''} t_{\alpha,L'L''} \sum_{\beta} G_{\alpha\beta,L''L}\phi^0_{\beta,L} \tag{1.111}$$

and $\phi^0_{\beta,L'} = \delta_{\beta\alpha_0}\varphi_{L'}$ are the direct wave coefficients, which are zero for atoms other than the emitter α_0.

This procedure can be repeated with each of the h_L components of Eq. (1.110) to lead to second-order scattering and so on. A recurrence relation can be obtained in this way, so that the coefficients of the expansion at order n can be obtained from those at order $n-1$ as

$$\phi^n_{\alpha,L} = \phi^0_{\alpha,L'} + \sum_{L'L''} t_{\alpha,LL''} \sum_{\beta\neq\alpha} G_{\alpha\beta,L''L'}\phi^{n-1}_{\beta,L'}, \tag{1.112}$$

where the restriction that $\beta \neq \alpha$ reflects the fact that the unscattered propagation from any atom to itself must be excluded.

In the $n \to \infty$ limit, Eq. (1.112) becomes a self-consistent secular equation,

$$\phi_{\alpha,L} = \phi^0_{\alpha,L'} + \sum_{L'L''} t_{\alpha,LL''} \sum_{\beta\neq\alpha} G_{\alpha\beta,L''L'}\phi_{\beta,L'}, \tag{1.113}$$

which has to be satisfied by the wave function components $\phi_{\alpha,L}$ of the photoelectron wave function

$$\phi(\mathbf{r}) = \sum_{\alpha} \sum_{L'} h_{L'}^{(+)}[k(\mathbf{r} - \mathbf{R}_\alpha)]\, \phi_{\alpha,L'} \tag{1.114}$$

outside the muffin-tin spheres.

From a numerical point of view, Eq. (1.113) can be approximated by a finite system of $N(l_{\max}+1)^2$ equations if one considers a cluster of N atoms and a maximum angular momentum number $l_{\max}$, which scales roughly as $l_{\max} \sim kr_{\mathrm{mt}}$ with the electron momentum k and the atomic muffin-tin radius r_{mt}. Unfortunately, the direct inversion of Eq. (1.113) is computationally very demanding and can be performed only for very limited cluster sizes and small values of $l_{\max}$ (low energies) [45]. Therefore, approximations have been introduced [90], some of them inspired by the high-energy limit, where the electron propagation reduces to plane-wave factors (plane-wave approximation) and each term in the MS series becomes a product of scattering amplitudes [7, 8, 62]. Beyond this, full curved-wave formulations of the problem have been also implemented [18, 26, 92].

Codes based upon the Rehr-Albers formalism make use of a convenient factorization of the path Green function into matrices that represent individual scattering events and that contain

curved wave effects up to any required accuracy (e.g., MSCD [18]); this results in a computation time that scales with the cube of the number of atoms in the cluster, but a path-cut can be introduced to reduce the computational demand drastically at the expense of small errors arising in the truncation of the multiple scattering series.

It is also possible to solve the multiple scattering equations without any approximation in the Green function by using iterative techniques based upon the recursion method. This is the procedure employed in EDAC [26], which presents the advantage of preventing any eventual lack of convergence in the multiple scattering. The computation time in this code scales with the square of the number of atoms, which allows calculations for clusters of up to several thousand atoms.

1.7 Matrix elements: core versus valence levels

The theoretical model introduced in Sec. 1.6.2 for calculating the photoelectron intensity from a core level can also be applied to study the photoemission from extended states, such as valence levels of molecules, clusters or solids. When the initial state of the electron is extended over several atoms, the initial wavefunction can be expanded as:

$$\Psi_i(\mathbf{r}) \;=\; \sum_{a}^{\text{emitters}} \sum_{L} \kappa_L^a \psi_L^a(|\mathbf{r}-\mathbf{r}_a|) Y_L(\Omega_{\mathbf{r}-\mathbf{r}_a}) \;. \tag{1.115}$$

In the latter equation, $\psi_L^a(\mathbf{r}-\mathbf{r}_a)$ are atomic orbitals centered about site a. The initial state is thus a combination of several atomic orbitals (hence the sum over L) at several sites (hence the sum over a). The factors κ_L^a are the coefficients of this linear combination.

Following a formalism similar to that of core-level photoemission, the wavefunction at the detector position $\phi(R_d)$ can be obtained as:

$$\phi(R_d) \;=\; \sum_{a}^{\text{emitters}} e^{-i\mathbf{k}\mathbf{r}_a} \sum_{L} \kappa_L^a \sum_{\alpha}^{\text{atoms}} \sum_{L'} \phi_{\alpha,L'}^{aL} \frac{e^{ik\mathrm{R}_d}}{k\mathrm{R}_d} Y_{L'}(\Omega_{R_d}) \;, \tag{1.116}$$

where the coefficients $\phi_{\alpha,L'}^{aL}$ now depend on L and a as well (the initial atomic orbital of quantum numbers L at emitter a), and the Hankel functions of Eq. (1.114) have been replaced by their asymptotic expansions. The final wavefunction (and consequently the photoelectron intensity at the detector position) is thus obtained as a coherent sum over emitters a with coefficients κ_L^a. An additional phase factor $e^{-i\mathbf{k}\mathbf{r}_a}$ accounts for the electron path difference between emitters. This assumes in-phase arrival of the incident photon wave at all emitter sites, namely an infinite photon wavelength; an additional phase factor can be inserted to account for a finite photon wavelength.

In the case of a perfect three-dimensional periodic lattice (for instance, an ideal infinite crystal without any surface), the initial state in the photoemission process can always be described as a Bloch state. In this case, the coefficients multiplying the atomic orbitals in Eq. (1.115) can be written in a different way, so that the Bloch condition is apparent:

$$\Psi_i(\mathbf{r}) \;=\; \sum_{a}^{\text{emitters}} e^{i\mathbf{k}\mathbf{r}_a} \sum_{L} K_L \psi_L^a(|\mathbf{r}-\mathbf{r}_a|) Y_L(\Omega_{\mathbf{r}-\mathbf{r}_a}) \;. \tag{1.117}$$

The new coefficients K_L do not depend on the site a because all sites are equivalent. They only depend on the quantum numbers L. The vector $\mathbf{k}$, which satisfies the Bloch condition, has the same dimensions of the periodic lattice. It does not change during the photoexcitation process (the electron momentum is conserved in the limit of an infinite photon wavelength). The final wavefunction at the detector position is then:

$$\begin{aligned}\Psi_f(R_d) &= \sum_a^{\text{emitters}} e^{i\mathbf{k}\mathbf{r}_a} \sum_L K_L \sum_\alpha^{\text{atoms}} \sum_{L'} \phi^{aL}_{\alpha,L'} \frac{e^{ik\mathrm{R}_d}}{k\mathrm{R}_d} e^{-i\mathbf{k}(\mathbf{r}_\alpha+\mathbf{r}_a)} Y_{L'}(\Omega_{R_d}) \\ &= \sum_a^{\text{emitters}} \sum_L K_L \sum_\alpha^{\text{atoms}} \sum_{L'} \phi^{aL}_{\alpha,L'} \frac{e^{ik\mathrm{R}_d}}{k\mathrm{R}_d} e^{-i\mathbf{k}\mathbf{r}_\alpha} Y_{L'}(\Omega_{R_d}) \\ &= \mathcal{N} \sum_L K_L \sum_\alpha^{\text{atoms}} \sum_{L'} \phi^{aL}_{\alpha,L'} \frac{e^{ik\mathrm{R}_d}}{k\mathrm{R}_d} e^{-i\mathbf{k}\mathbf{r}_\alpha} Y_{L'}(\Omega_{R_d}) \,. \end{aligned} \tag{1.118}$$

In the latter equation $\mathcal{N}$ is a normalization constant arising from the sum over equivalent lattice sites, with no important role in the calculation of the intensity. Eq. (1.118) shows that, for a 3D periodic system, the final wavefunction (and consequently the photoelectron intensity at the detector position) can be evaluated by calculating the photoelectron intensity *from one single site* a; more generally, from all those sites that are translationally inequivalent within a unit cell. Every single equivalent site of the lattice emits coherently but there is no phase shift among the photoemission processes from different equivalent sites for an infinite photon wavelength. A similar formalism can be developed for a system in which there is periodicity in only two dimensions. Then emitters at different depths are no longer equivalent and their emission must be considered separately, but still coherently.

For a finite photon wavelength, the photon path differences among different emitters must be included in the previous equations. Especially for very large systems, such as with infinitely extended initial states, an additional phase factor, depending on the emitter position and on the light wavevector, will thus appear in Eq. (1.118).

1.8 optical effects

Generally, the photons can be dressed by any type of excitation that they are able to produce in a solid (e.g., plasmons, phonons, and all kind of quasiparticles).

Screening of the external light is important for photoemission from solids, specially at low photon energies, and in particular near the plasmon energy, in which case the medium induces an electric field that can be comparable in magnitude to the external field provided by the light near the surface. It then can be also comparable in wavelength with the atomic spacing.

Strong variations of the electric field near the surface can play a substantial role in the so-called surface emission, which has been clearly observed in angle resolved photoemission [86], and that is relatively well described by the Fresnel equations [63], which requires knowledge of the dielectric function of the solid material. The latter can be obtained from experiment. In particular, for low photon energies (e.g., < 50 eV) complex collective excitations (e.g., plasmons) dominate the response. At these low energies, the photon wavelength (> 24

nm) is much larger than the typical surface lattice constant, and therefore, principally the medium should be well described by its macroscopic, frequency-dependent dielectric function, which neglects all kind of details on the atomic scale. But as it will be outlined in subsection 1.8.2, induced local fields yield important perturbations on a lattice scale near the plasmon frequency.

1.8.1 Resonant photoemission

Resonant photoemission is an interesting phenomenon which takes place when the photon energy is tuned to a resonance of the emitting atoms. Then, the photoelectron has two different emission channels: (i) direct excitation by absorbing an external photon and (ii) excitation of the resonance followed by its decay while the excess of energy is carried away by the photoelectron. These two different quantum channels leave the sample in exactly the same final state, and thus, they have to be added coherently, leading to interference effects that in general follow Fano profiles [29].

This phenomenon can be considered to be a screening effect: the external photon is dressed by interaction with a many-body system that is able to hold localized excitations (the atomic resonance), similar to excitons in solids. This is particularly important at low incidence angles, which can limit the penetration depth of the light dramatically, especially in metals, where the so-called skin depth of visible and near UV light is only a few nanometers. Also, dramatic effects have been observed under total reflection conditions [52, 84].

At higher photon energies (e.g., > 100 eV), the response is governed by the X-ray scattering factors of the solid atoms, so that the screening at those energies comes primarily from dynamical X-ray scattering. Besides, the *effective* dielectric function at those energies is very close to 1, since the response is small. However, some effects can be observed at the energies of the absorption edges. More precisely, when the external light is tuned at the energy of an absorption resonance of one of the atoms in the solid, strong induced fields comparable in magnitude with the external field are produced, especially at low incidence angles. This has been recently observed in photoemission from O 1s in MnO illuminated with light near the Mn2p absorption edge (640 eV) [25, 66, 67]. The O 1s photoelectron signal showed a strong modulation near that photon energy, and this has been explained in terms of the Mn resonating atoms, which suffer virtual excitations by the incoming light to decay later while transferring the excitation energy to O 1s electrons.

This is the so-called multi-atom resonant photoemission (MARPE), which provides a way to identify the chemical nature of neighboring atoms in a solid, since the resonance energy is a characteristic of one kind of atoms while the observed photoelectrons are emitted from a different kind of atoms. An example of this if offered in Fig. 1.13 for emission from oxygen near the Mn2p absorption edge in MnO [25, 66, 67]. The theory in this figure is based upon first principles calculation of the atomic polarizability of Mn in MnO and multiple scattering of photons in between different Mn scatterers. The result of this multiple scattering produces an effect that can be also explained in terms of a dielectric model (using Clausius-Mossotti to convert the Mn polarizability into dielectric function), where the emission intensity maps the square of the external electric field at the surface region.

A very good agreement has been obtained between theory and experiment in this latter case, and also between a microscopic theory of the solid response based upon first principles

calculations of the atomic scattering factors as compared with a macroscopic description using Fresnel's equations and the dielectric function derived from the Clausius-Mossotti relation.

Beyond this simple model, *ab initio* theories have been developed to compute the response function of the solid, although severe approximations have to be made in order to cope with the complexity of the surface. These models take into consideration the detailed bandstructure of the solid in order to construct the response function. In the simplest scheme, one simply uses one-electron wave functions to obtain the RPA susceptibility [59]. While this approach generally gives good results for metals, several problems emerge when it is applied to insulators: excitons are not described at all and one needs to go beyond the RPA and use the Bethe-Salpeter equation for a correct description of electron-hole pairs [33].

1.8.2 Photoemission by surface optical response fields

The assumptions in Eq. (1.89), with respect to periodicity as well as to long wavelength, must be questioned if the response of the emitting material to the incident light adds induced fields capable of appreciable separate excitations. Such fields change on a length scale of the lattice constant because they originate from the ionic polarizability, and they are non-periodic because of the surface. These effects become important for a small real part of the dielectric function $\epsilon(\mathbf{r}, \mathbf{r}', \omega)$ implying large fields for even small amplitude external light which might occur especially for ω near the plasmon frequency.

Because of their short wavelength these fields are denoted as "local fields" well known from optics: they drastically change the homogeneous dielectric constant $\epsilon_0(\omega)$ from its microscopic to the macroscopic observable value. The surface adds nonlocality to ϵ as stressed by noting the dependence on two local variables $\mathbf{r}, \mathbf{r}'$. It arises e.g. from surface scattering of the electromagnetic wave and from further enhancement by plasmon generation. Though both effects are well known in the literature, (the latter especially has been first observed in connection with photoemission [73]), the full incorporation into one-step photoemission calculations

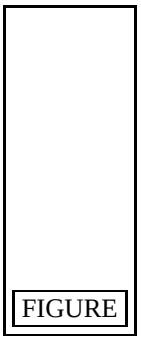

Figure 1.13: Multi-atom resonant photoemission in MnO(100) surfaces. **(a)** A photon can produce photoemission from an O atom, but in a different channel the same photon can excite a Mn atom of the sample, which decays transfering its energy to the first O atom. The final state in both channels is the same, so that they have to be added coherently. **(b)** Measured absorption spectrum near the Mn2p edge, showing the energies where Mn can actually be efficiently excited. **(c)** O1s photoelectron intensity within the Mn2p resonance energy range.

is still lacking. A few calculations include the dielectric function in the determination of the photocurrent, but use more or less heuristic models. Two examples applying to solids will be described in the following (further details may be found in Ref. [97]): In particular, optical investigations carry more information about local fields [71] and surface response [76].

Local fields are conveniently illustrated in layered crystals, e.g. in $TiSe_2$ where they appear as polarization fields perpendicular to the layers, i.e. parallel to the axis of the valence Se-p_z orbitals across the layers. Thus, the induced field will couple to that orbital leading to additional photoemission from it. Quantitatively, the vector potential $\mathbf{A}$ in Eq. (1.87) must be replaced by

$$\mathbf{A}_{\mathbf{G}}(\omega) = (\epsilon^{-1})_{\mathbf{G}0}\,\mathbf{A}_{\mathbf{0}}^{\text{ext}}(\omega) \tag{1.119}$$

where $\mathbf{A}^{\text{ext}}$ refers to the incident external light, $\mathbf{G}$ denotes a reciprocal lattice vector, and (ϵ^{-1}) refers to the matrix element with respect to the two vector indices $\mathbf{G}$ and $\mathbf{0}$. Here, the incident wavelength is assumed long compared to the lattice spacing, which is valid up to the vacuum ultraviolet regime. Values for ϵ must be taken from separate optical calculations. They show a strong enhancement near the plasma frequency, i.e. around 20 eV for $TiSe_2$, which can cause 100% changes in the photocurrent, leading to a dominating peak for the Se-p_z emissions. The reciprocal lattice vector $\mathbf{G}$ of the prominent induced-light component is $2\pi/c$ [0001], the first non-zero vector perpendicular to the layers corresponding to a wavelength equal to the perpendicular lattice spacing c. [10]

Nonlocal response also has been investigated for layered materials. Owing to the lack of any general ab-initio determination of the surface response, the hydrodynamic model of the bulk electron gas may give a first impression of the induced longitudinal plasmon waves and the correspondingly longitudinal response fields for photons above the plasmon frequency. Because of the boundary conditions, the induced field points perpendicularly to the surface and propagates into the interior of the solid. It varies locally on a scale involving the valence electron density and the difference between light and plasma frequency: the induced field increases when the plasma frequency increases and the light frequency decreases. Again, the corrected field is introduced into the photoemission calculation via Eq. (1.119). [95] Similar to the above case, the additional field can excite Se-p_z emissions, also yielding a 100% enhancement of the photocurrent close to the plasma frequency above it. [95]

This topic is now still developing from its rather model-like state, depending on the growth in computer power. The effect on the electron distribution curves of photoemission can be extremely large, such that its neglect produces doubtful peak heights and peak positions under the above circumstances of observation. In Fig. 1.14 the high significance of these effects becomes apparent. A structure dispersing between 0 and -2 eV which consists mainly of p_z orbitals is enhanced by including the local fields induced by the incident photon in contrast to the non-dispersive peak at -3 eV. The experiment reveals that the theory overestimates this effect which, of course, is related to the crude approach of using the bulk dielectric matrix for the local fields.

An ab-initio calculation of the full dielectric matrix function for semi-infinite systems has been completed recently. [16] Its application to photoemission with the aim considered here is in progress.

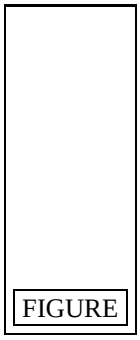

Figure 1.14: Theoretical photoelectron spectra at left, including (solid) and neglecting (broken) local fields, for normal emission from $TiSe_2(0001)$ with bandstructure plotted on top, compared with experimental spectra [4] at right; photon energy as parameter at the curves

1.9 Spin effects

The spin of the electron plays an important role in photoemission from magnetic atoms or when states that suffer strong spin-orbit coupling are involved. Normal detectors do not discriminate between spin polarization of the photoelectrons, unless strongly spin-polarized initial states are considered [101,106]. However, the increasing enhancement in photon flux from new generations of synchrotrons and free-electron lasers are making it possible to collect reasonable signals using spin-selective Mott detectors, where the electron detection efficiency is low since spin separation is performed by tiny differences in the angular distribution of Mott scattering of photoelectrons at the detector.

Magnetic samples define a category of experiments where spin is important. Common techniques in this context involve measuring magnetic dichroism, that is, the fractional change in photoelectron intensity either when the magnetization of the sample is reversed [54] or when the light polarization is changed (e.g., from left to right circularly polarized light [101]).

From an atomic point of view, the magnetic dichroism signal in core-level photoemission permits establishing the magnitude of spin-orbit coupling in the final state of the ionized emitting atom [100]. It also provides quantitative information on the magnetic moment of oriented magnetic atoms, and can be used to determine Curie and Néel temperatures near the surface of the material from which the photoelectron originates (these temperatures may differ from the bulk values [106]).

Spin effects are to some extent a reflection of the initial and final states of the emitting atom, which can be generally described by one-electron states in the case of closed shells (e.g., in emission from Fe2p or Gd4d [100]). General open shell configurations however involve complex many-electron states, which result in photoemission spectra composed of many multiplet lines.

Multiple scattering of the photoelectron introduces additional spin dependence originating in the different scattering properties of electrons polarized either parallel or antiparallel with respect to the magnetic moment of the atoms [53,106]. Besides, spin-orbit coupling effects in photoelectron scattering from solid atoms (Mott scattering) can play an important role even in

the VUV region. This is particularly true along scattering directions of strong spin anisotropy when they coincide with atomic bonds that produce forward focusing effects. These effects introduce spin dependence in multiple scattering for non-magnetic atoms as well [102].

Spin effects can be easily implemented in the multiple scattering scheme discussed in Sec. 1.6.2. In particular, the atomic scattering matrix needs to be supplemented by the electron spin quantum number. In magnetic atoms with negligible spin-orbit coupling, the scattering matrix can be split into disconnected spin-up and spin-down pieces, each of which is described by the corresponding atomic potential that takes into account exchange and correlation effects [108]. When spin-orbit coupling is included, a complex interplay with magnetic exchange leads to dense scattering matrices [102, 103]. Finally, the propagation of the electron in the muffin-tin interstitial potential can be performed in the same way as in Sec. 1.6.2, independently for each spin component. These possibilities are contemplated in the EDAC code [25] (see Sec. 1.10)".

1.10 Computer codes for photoelectron diffraction and spectroscopy

A variety of computer codes have been written to simulate photoelectron diffraction. A majority of these codes were designed for surface structure determination, similar to LEED codes. This often includes some form of automatic fitting of structural parameters such as atomic coordinates that affect interlayer spacings or bond lengths near the surface. Other codes aim to study different aspects of surfaces, including magnetic or relativistic effects, electronic band-structure and/or the spatial distribution of electrons.

We here discuss and compare several codes for which we have detailed information (a number of other codes exist):

- MSPHD by R. Gunnella, C.R. Natoli, F. Solal and D. Sébilleau (superfici.unicam.it/photoelectron_diffraction.htm)
- SPEC by D. Sébilleau;
- PRAPD by M.D. Pauli, H.C. Poon, D.K. Saldin and A. Wander (giotto.phys.uwm.edu) – this code also models Auger electron diffraction;
- 'Fritzsche' (as we will call this code, since it does not appear to have an established name) by V. Fritzsche;
- MSCD by Y. Chen, M.A. Van Hove, C.S. Fadley, F. Bondino and R. Díez Muiño (http://electron.lbl.gov/mscdpack/mscdpack.html);
- EDAC by F.J. García de Abajo, M.A. Van Hove and C.S. Fadley (http://electron.lbl.gov/edac, http://csic.sw.ehu.es/edac);
- ZBE110 by J.-V. Peetz and W. Schattke (http://www.theo-physik.uni- kiel.de/theo-physik/schattke/);

- KSAP by T. Strasser, C.-H. Solterbeck, J. Henk, A. Bödicker and W. Schattke (http://www.theo-physik.uni-kiel.de/theo-physik/schattke/);

- ISOLDA by E.E. Krasovskii, F. Starrost, O. Tiedje and W. Schattke (http://www.theo-physik.uni-kiel.de/theo-physik/schattke/).

The codes can be distinguished according to their basic geometric approach: atomic clusters of various shapes and sizes vs. two-dimensionally periodic surfaces of variable depth. As with electronic structure calculations at surfaces, the relative advantages and disadvantages of these two fundamental choices have been hotly debated. For core-level emission, in which a single atom emits waves of spherical character (since other atoms emit incoherently), the cluster approach is intuitive: it is used by MSPHD, SPEC, Fritzsche, MSCD and EDAC. For core- level emission, the periodic-surface model requires thinking in terms of 'inverse LEED states', so that plane waves become prominent and LEED-like layer-by-layer methods become applicable, as used in PRAPD, ZBE110 and KSAP.

Very few photoelectron diffraction codes can now handle valence-level emission; exceptions are KSAP and ISOLDA. With valence levels, the initial state is a molecular or band state that extends over several atoms or an infinite number of atoms. Photoemission from such a state can be viewed as the coherent superposition of atomic-like emissions, and this can be done within either a cluster model or a periodic-surface model; the latter has clear advantages for dealing with infinitely extended valence bands and resembles the current highly-developed bandstructure codes. As the photoemission final states are not accessible by these bandstructure codes, an independent confirmation through VLEED or TCS in this energy domain deserves interest. Such information is supported by calculations via codes such as ZBE110 because of their full-potential capability.

The different codes generally can model the various standard modes of data collection: polar and azimuthal scans, hemispherical scans, energy-dependent scans, and combinations of these. Most codes also accept both linear-polarized and unpolarized light, while a few allow circular and elliptical polarization of the incident light (MSCD, EDAC).

However, very few codes consider the effect that the surface has on the incident radiation itself: its refraction, change of polarization, attenuation, etc. KSAP is an exception, since it includes these effects via the input.

The photoexcitation is normally treated in the Golden Rule approximation, assuming the dipole and sudden approximations (MSPHD uses the $Z + 1$ approximation). With EDAC and KSAP, non-dipole effects can be included through an input file.

Relativistic and magnetic effects are usually only allowed to the extent that the electron scattering phase shifts that are input from an external source include relativistic effects. EDAC explicitly includes both relativistic and magnetic effects through spin-dependent phase shifts and scattering amplitudes, yielding for instance spin polarization. Furthermore, this code is fully automated, and in particular, scattering phase shifts and excitation matrix elements are calculated internally without the need for further input.

Many schemes for treating photoemission either by multiple scattering or by direct solution of the Schrödinger equation have been programmed: each code seems to use a different formulation. However, it is accepted that all these schemes can converge to the same correct result if brought to full convergence, even though there are cases of divergence. Since in prac-

tice each scheme is truncated due to limits on computer size and especially computing time, some small differences in results are inevitable.

Inelastic effects (energy losses of the emitted electrons) are accounted for by one of two schemes: complex phase shifts that include the loss process in the atomic scattering (MSPHD, SPEC); or attenuation of the waves propagating from atom to atom with elastic atomic scattering (all other codes). Attenuation can be described either as a mean free path or as an imaginary component of the constant potential outside the atoms. In the direct solution of the Schrödinger equation a complex optical potential is applied throughout space.

The effect of vibrations is mostly modeled through an uncorrelated Debye-Waller factor acting at each scattering in a multiple-scattering path. Some codes neglect the effect altogether (MSPHD, KSAP); others include a correlated Debye-Waller factor (MSCD) which takes into account that the vibrations of nearby atoms are partly correlated, so that the apparent vibrations are less strong as seen by an electron scattering in succession from nearby atoms.

The emitted electron has to pass the potential barrier step between solid and vacuum. This is usually treated only as a refractive effect (with no reflection), but it is neglected in MSPHD: refraction makes an electron change its propagation direction due to its change of momentum perpendicular to the surface. In KSAP and ISOLDA, this effect is included to any desired accuracy, including reflection.

The computational time requirements of the different codes have various scaling laws as a function of the problem size: these scaling laws depend strongly on the particular algorithm used to perform the multiple scattering. The time requirements normally grow significantly with increasing electron energy, and with the number of inequivalent atoms. For instance, PRAPD scales roughly as g^{2N}, where g is the number of plane waves used and N is the number of atomic planes present in the surface slab of finite thickness. MSCD and EDAC scale as N^3 and N^2, respectively, if N is the number of atoms present in the cluster. KSAP and ISOLDA scale as N^3 with N being the number of atoms per surface unit cell of the semi-infinite system.

Most codes are written in Fortran, and are generally run under Unix or Linux. MSCD and EDAC are written in C++, having versions for PC, Mac, Unix and parallel machines (this one only for MSCD).

The degree of availability, documentation and support of the different codes varies widely: one should consult with the respective authors for details. MSPHD is available through Computer Physics Communications. SPEC has short documentation and in-house training. PRAPD is well documented and training is available. One may download MSCD with its extensive documentation. A demo version of EDAC may be interactively run on the web, while its full version is to appear in Computer Physics Communications. KSAP, ISOLDA and ZBE110, with brief comments, are available on the web.

Acknowledgements

Parts of this chapter strongly benefit from cooperation with C.-H. Solterbeck. This work was supported by the Director, Office of Science, Office of Basic Energy Sciences, Division of Materials Sciences and Engineering, of the U.S. Department of Energy under Contract No. DE-AC03-76SF00098, by the Bundesministerium für Bildung, Wissenschaft, Forschung und Technologie (BBWFT) under contract Nos. 05 5FKTAB 1 and 05 605FKA 1, by the Basque

Departamento de Educación, Universidades e Investigación, the University of the Basque Country UPV/EHU (9/UPV 00206.215-13639/2001), and the Spanish Ministerio de Ciencia y Tecnología (MAT2001-0946). RDM acknowledges financial support by the Gipuzkoako Foru Aldundia (Gipuzkoa Fellows Program).

References

[1] B. Ackermann and R. Feder. *Solid State Communications*, 54:1077, 1985.
[2] B. Ackermann and R. Feder. *Journal of Physics C*, 18:1093, 1985.
[3] C.-O. Almbladh. *Physica Scripta*, 32:341, 1985.
[4] O. Anderson. PhD thesis, Christian-Albrechts-Universität zu Kiel, 1986.
[5] G.B. Bachelet, D.M. Ceperley, and M.G.B. Chiocchetti. *Phys. Rev. Lett.*, 62:2088, 1989.
[6] A. Bansil and M. Lindroos. *Phys. Rev. Lett.*, 83:5154, 1999.
[7] J.J. Barton and D.A. Shirley. *Phys. Rev. A*, 32:1019, 1985.
[8] J.J. Barton and D.A. Shirley. *Phys. Rev. B*, 32:1906, 1985.
[9] C.N. Berglund and W.E. Spicer. *Phys. Rev.*, 136:A1030, 1964.
[10] A. Bödicker, A. Leventi-Peetz, and W. Schattke. *J. El. Spectrosc. and Relat. Phenomena*, 78:481, 1996.
[11] A. Bödicker and W. Schattke. *Phys. Rev. B*, 55:5045, 1997.
[12] D. Bohm and D. Pines. *Phys. Rev.*, 92:609, 1953.
[13] S.V. Borisenko, M.S. Golden, S. Legner, T. Pichler, C. Dürr, M. Knupfer, J. Fink, G. Yang, S. Abell, and H. Berger. *Phys. Rev. Lett.*, 84:4453, 2000.
[14] J. Braun, G. Thörner, and G. Borstel. *physica status solidi (b)*, 130:643, 1985.
[15] J. Braun, G. Thörner, and G. Borstel. *physica status solidi (b)*, 144:609, 1987.
[16] S. Brodersen and W. Schattke. *Phys. Rev. B*, 66:153303, 2002.
[17] C. Caroli, D. Lederer-Rozenblatt, B. Roulet, and D. Saint-James. *Phys. Rev. B*, 8:4552, 1973.
[18] Y. Chen, F.J. García de Abajo, A. Chassé, R.X. Ynzunza, A.P. Kaduwela, M.A. Van Hove, and C.S. Fadley. *Phys. Rev. B*, 58:13121, 1998.
[19] Y.-D. Chuang, A.D. Gromko, D.S. Dessau, Y. Aiura, Y. Yamaguchi, K. Oka, A.J. Arko, J. Joyce, H. Eisaki, S.I. Uchida, and Yoichi Ando K. Nakamura. *Phys. Rev. Lett.*, 83:3717, 1999.
[20] R. Claessen, R.O. Anderson, J.W. Allen, C.G. Olson, C. Janowitz, W.P. Ellis, S. Harm, M. Kalning, R. Manzke, and M. Skibowski. *Phys. Rev. Lett.*, 69:808, 1992.
[21] H. Daimon, F. Matsui, and K. Sakamoto. *this volume*.
[22] A. Derevianko, O. Hemmers, S. Oblad, P. Glans, H. Wang, S.B. Whitfield, R. Wehlitz, I.A. Sellin, W.R. Johnson, and D.W. Lindle. *Physical Review Letters*, 84:2116, 2000.
[23] S.S. Dhesi, C.B. Stagarescu, K.E. Smith, D. Doppalapudi, R. Singh, and T.D. Moustakas. *Phys. Rev. B*, 56:10271, 1997.
[24] O. Heinonen E.K.U. Gross, and E. Runge. *Many-Particle Theory*. Adam Hilger, 1991.
[25] F.J. García de Abajo, C.S. Fadley, and M.A. Van Hove. *Phys. Rev. Lett.*, 82:4126, 1999.

[26] F.J. García de Abajo, M.A. Van Hove, and C.S. Fadley. *Phys. Rev. B*, 63:075404, 2001.

[27] C.S. Fadley, Y. Chen, R.E. Couch, H. Daimon, R. Denecke, J.D. Denlinger, H. Galloway, Z. Hussain, A.P. Kaduwela, Y.J. Kim, P.M. Len, J. Liesegang, J. Menchero, J. Morais, J. Palomares, S.D. Ruebush, E. Rotenberg, M.B. Salmeron, R. Scalettar, W. Schattke, R. Singh, S. Thevuthasan, E.D. Tober, M.A. Van Hove, Z. Wang, and R.X. Ynzunza. *Progr. Surf. Sci.*, 54:341, 1997.

[28] C.S. Fadley, See-Hun Yang, Bongjin Simon Mun,and F.J. García de Abajo. *this volume*.

[29] U. Fano. *Phys. Rev.*, 124:1866, 1961.

[30] R. Feder and H. Gollisch. *this volume*.

[31] P.J. Feibelman and D.E. Eastman. *Phys. Rev. B*, 10:4932, 1974.

[32] P.J. Feibelman and D.E. Eastman. *Physical Review B*, 10:4932, 1974.

[33] A.L. Fetter and J.D. Walecka. *Quantum Theory of Many-Particle systems*. McGraw Hill, New York, 1971.

[34] B. Feuerbacher, B. Fitton, and R.F. Willis. *Photoemission and Electronic States Properties of Surfaces*. Wiley, Chichester, 1978.

[35] A. Fleszar and W. Hanke. *Phys. Rev. B*, 62:2466, 2000.

[36] N. Fominykh, J. Berakdar, J. Henk, S. Samarin, A. Morozov, F.U. Hillebrecht, J. Kirschner, and P. Bruno. *this volume*.

[37] A.J. Freeman, R. Asahi, A. Continenza, and R. Wu. *this volume*.

[38] H.M. Fretwell, A. Kaminski, J.C. Campuzano J. Mesot, M.R. Norman, M. Randeria, T. Sato, R. Gatt, T. Takahashi, and K. Kadowaki. *Phys. Rev. Lett.*, 84:4449, 2000.

[39] G.D.Mahan and E.W.Plummer. *Handbook of Surfaces, II: Electronic Structure of Surfaces*. ed. K. Horn and M. Scheffler, Elsevier-North Holland, 1995.

[40] B. Ginatempo, P.J. Durham, and B.I. Gyorffy. *Journal of Physics C*, 17:6483, 1989.

[41] M.L. Goldberger and K.M. Watson. *Collision Theory*. Wiley, New York, 1964.

[42] A. Gonis and W.H. Butler. *Multiple Scattering in Solids*. Springer, New York, 2000.

[43] T. Grandke, L. Ley, and M. Cardona. *Phys. Rev. B*, 18:3847, 1978.

[44] M. Graß, J. Braun, and G. Borstel. *Physical Review B*, 47:15487, 1993.

[45] R. Gunnella, F. Solal, D. Sebilleau, and C.R. Natoli. *Computer Phys. Comm.*, 132:251, 2000.

[46] S.V. Halilov, E. Tamura, H. Gollisch, D. Meinert, and R. Feder:. *Journal of Physics Condensed Matter*, 5:3859, 1993.

[47] R.J. Harder and D.K. Saldin. *this volume*.

[48] S. Harm, R.Dürig, R. Manzke, M. Skibowski, R. Claessen, and J.W. Allen. *J. Electron. Spectrosc. & Relat. Phenom.*, 68:111, 1994.

[49] L. Hedin. *this volume*.

[50] L. Hedin. *J. Phys.: Condens. Matter*, 11:R489, 1999.

[51] L. Hedin. *arXiv:cond-math, 27Sep2001*, page 0109517, 2001.

[52] B.L. Henke. *Phys. Rev. A*, 6:1972, 1972.

[53] B. Hermsmeier, J. Osterwalder, D.J. Friedman, B. Sinkovic, T. Tran, and C.S. Fadley. *Phys. Rev. B*, 42:11895, 1990.

[54] F.U. Hillebrecht, H.B. Rose, T. Kinoshita, Y.U. Idzerda, G. van der Laan, R. Denecke, and L. Levy. *Phys. Rev. Lett.*, 75:2883, 1995.

[55] F.J. Himpsel and K.N. Altmann. *this volume*.

[56] P. Hohenberg and W. Kohn. *Phys. Rev. B*, 136:864, 1964.

[57] J.F.L. Hopkinson, J.B. Pendry, and D.J. Titterington. *Computer Physics Communications*, 19:69, 1980.

[58] M.A. Van Hove and S.Y. Tong. *Surface Crystallography by LEED*. Springer, Heidelberg, 1979.

[59] M.S. Hybertsen and S.G. Louie. *Phys. Rev. B*, 34:5390, 1986.

[60] P. Fulde. *Electron Correlation in Molecules and Solids*. Springer Series in Solid-State Sciences, Vol. 100, 1991.

[61] J.K. Inkson. *The Many-Body Theory of Solids*. Plenum Press, New York, 1984.

[62] J. Mustre de Leon, J.J. Rehr, C.R. Natoli, C.S. Fadley, and J. Osterwalder. *Phys. Rev. B*, 39:5632, 1989.

[63] J.D. Jackson. *Classical Electrodynamics*. Wiley, New York, 1999.

[64] L.P. Kadanoff and G. Baym. *Quantum Statistical Mechanics*. Benjamin, New York, 1962.

[65] E.O. Kane. *Physical Review Letters*, 12:97, 1964.

[66] A. Kay, E. Arenholz, S. Mun, F.J. García de Abajo, C.S. Fadley, R. Denecke, Z. Hussain, and M.A. Van Hove. *Science*, 281:679, 1998.

[67] A. Kay, F.J. García de Abajo, S.-H. Yang, E. Arenholz, S. Mun, N. Mannella, Z. Hussain, M.A. Van Hove, and C.S. Fadley. *Phys. Rev. B*, 63:115119, 2001.

[68] L.V. Keldysh. *J. Exptl. Theoret. Phys.*, 47:1515, 1964.

[69] W. Kohn and L.J. Sham. *Phys. Rev. A*, 140:1133, 1965.

[70] E.E. Krasovskii. *this volume*.

[71] E.E. Krasovskii and W. Schattke. *Phys. Rev. B*, 63:235112, 2001.

[72] E.E. Krasovskii, W. Schattke, V.N. Strocov, and R.Claessen. *Phys. Rev. B*, 66:235403, 2002.

[73] H.J. Levinson and E.W. Plummer. *Phys. Rev. B*, 24:628, 1981.

[74] A. Liebsch. *Phys. Rev. B*, 13:544, 1976.

[75] A. Liebsch. *Theoretical aspects of photoemission in Festkörperprobleme ed. J. Treusch*, volume XIX. Vieweg, Braunschweig, 1979.

[76] A. Liebsch. *Electronic excitations at metal surfaces*. Plenum, New York, 1997.

[77] J. Lindhard. *Dan. Vidensk. Selsk. Mat. Fys. Medd.*, 28:8, 1954.

[78] M. Lindroos, S. Sahrakorpi, and A. Bansil. *Phys. Rev. B*, 65:054514(1), 2002.

[79] S. Lorenz, C.-H. Solterbeck, W. Schattke, J. Burmeister, and W. Hackbusch. *Phys. Rev. B*, 55:R13432, 1997.

[80] G.D. Mahan. *Many Particle Physics*. Plenum, New York, 1981.

[81] S.T. Manson and D. Dill. *Electron Spectroscopy: Theory, Techniques and Applications*. Ed. by C.R. Brundle and A.D. Baker, Academic Press, London, New York, San Francisco, 1978.

[82] G. Margaritondo, D.L. Huber, and C.G. Olson. *Science*, 246:770, 1989.

[83] R.D. Mattuck. *A Guide to Feynman Diagrams in the Many Body Problem*. Dover, 1992.

[84] M. Mehta and C.S. Fadley. *Phys. Lett. A*, 55:59, 1975.

[85] A. Messiah. *Quantum Mechanics*. North-Holland, New York, 1966.

[86] T. Michalke, A. Gerlach, K. Berge, R. Matzdorf, and A. Goldmann. *Phys. Rev. B*, 62:10544, 2000.

[87] C.R. Natoli, M. Benfatto, C. Brouder, M.F. Ruiz López, and D.L. Foulis. *Phys. Rev. B*, 42:1944, 1990.

[88] R. Nozawa. *J. Math. Phys.*, 7:1841, 1966.

[89] J.-V. Peetz, W. Schattke, H. Carstensen, R. Manzke, and M. Skibowski. *Physical Review B*, 46:10127, 1992.

[90] J.B. Pendry. *Low Energy Electron Diffraction*. Academic Press, London, 1974.

[91] J.B. Pendry. *Surf. Sci.*, 57:679, 1976.

[92] J.J. Rehr and R.C. Albers. *Phys. Rev. B*, 41:8139, 1990.

[93] P. Roman. *Advanced Quantum Theory*. Addison-Wesley, Reading, 1965.

[94] K. Roßnagel and L. Kipp. *this volume*.

[95] D. Samuelsen, E. Pehlke, W. Schattke, O. Anderson, R. Manzke, and M. Skibowski. *Phys. Rev. Lett.*, 68:522, 1992.

[96] W.L. Schaich. *Photoemission in Solids I, 105*. ed. M. Cardona, 1978.

[97] W. Schattke. *Progr. Surface Sci.*, 54:211, 1997.

[98] W. Schattke. *Progr. Surface Sci.*, 64:89, 2000.

[99] L.J. Sham and M. Schlüter. *Phys. Rev. Lett.*, 51:1888, 1983.

[100] K. Starke. *Magnetic Dichroism in Core-Level Photoemission*, volume 159. Springer Tracts in Modern Physics, Berlin, 2000.

[101] K. Starke, A.P. Kaduwela, Y. Liu, P.D. Johnson, M.A. Van Hove, C.S. Fadley, V. Chakarian, E.E. Chaban, G. Meigs, and C.T. Chen. *Phys. Rev. B*, 53:R10544, 1996.

[102] P. Strange. *Relativistic Quantum Mechanics*. Cambridge University Press, Cambridge, 1998.

[103] P. Strange, J. Staunton, and B.L. Gyorffy. *J. Phys. C*, 17:3355, 1984.

[104] V.N. Strocov, H. Starnberg, P.O. Nilson, H.E. Brauer, and L.J. Holleboom. *Phys. Rev. Lett.*, 79:467, 1997.

[105] G. Thörner and G. Borstel. *physica status solidi (b)*, 126:617, 1984.

[106] E.D. Tober, F.J. Palomares, R.X. Ynzunza, R. Denecke, J. Morais, Z. Wang, G. Bino, J. Liesegang, Z. Hussain, and C.S. Fadley. *Phys. Rev. Lett.*, 81:2360, 1998.

[107] S.Y. Tong and M.A. Van Hove. *Sol. St. Comm.*, 19:543, 1976.

[108] U. von Barth and L. Hedin. *J. Phys. C*, 5:1629, 1972.